Fakultät für Medizin

Klinik für Plastische Chirurgie und Handchirurgie

Evidence of an unreported cell relationship responsible for linear collagen of triple negative breast tumors

Elizabeth Anne Brett

Vollständiger Abdruck der von der Fakultät für Medizin der Technischen Universität München zur Erlangung des akademischen Grades eines

Doctor of Philosophy (Ph.D.)

genehmigten Dissertation.

Vorsitzender: Prof. Dr. Roland M. Schmid

Betreuer: Prof. Dr. Hans-Günther Machens

Prüfer der Dissertation:

1. Prof. Dr. Achim Krüger

2. Priv.-Doz. Dr. Georg M. Huemer

Die Dissertation wurde am 16.06.2020 bei der Fakultät für Medizin der Technischen Universität München eingereicht und durch die Fakultät für Medizin am 10.09.2020 angenommen.

Abstract

The triple-negative breast tumor border is well-documented as a striated boundary, with linear ECM leading away from the tumor body. While it is known that linear collagen is pro-oncogenic, there is no explanation available on its formation. This thesis will focus on understanding and filling this knowledge gap. A tumor border is simulated *in vitro* by co-culturing fibroblasts, adipose derived stem cells, and MDA-MB-231 cells. Decellularization after one week reveals a linear extracellular matrix made chiefly of collagen type VI, which enhances invasion of reseeded cells. Further investigation shows that a juxtacrine culture of adipose derived stem cells and MDA-MB-231 creates high levels of CCL5, to which the fibroblasts react by producing pro-oncogenic, linear collagen VI. Inhibiting CCL5 within the co-culture results in an extracellular matrix which contains significantly less collagen VI, and is unorganized. Congruently, invasion of reseeded cells is not enhanced. In conclusion, these data represent an unreported axis between cell types of triple negative breast cancer. Specifically, cancer-derived CCL5 acts on fibroblasts in a paracrine manner, which stimulates production of linearized collagen.

Lay summary

Invasive breast cancer is extremely common as a type of breast cancer diagnosed every year. It is characterized by a metastatic tumor, sometimes spread to lymph nodes and other organs like the lung and brain. The original tumor in the breast has an outer shell with very thin, spiny extensions of collagen pointing outwards into the healthy breast. These threads of collagen mark the transformation of a non-invasive tumor to a metastatic body; expanding the range of the tumor and allowing access to blood vessels. There are multiple collagen types in the body, however, these spiny outgrowths contain a high amount of collagen type VI. The work of this PhD has been to establish which cells make the linear collagen VI, and the chemical messengers which instruct the cells to do so. This project has shown that a molecule called CCL5 is pivotal to the construction of linear collagen by healthy cells of the breast and breast cancer cells working together. Applying this work to the hospital situation, blocking CCL5 in patients

with breast cancer may stop the tumor from creating the invasive outer border of linear collagen, and presents a new, unexplored treatment option.

Introduction

Materials and methods

Results

List of figures

List of tables

List of abbreviations

ANOVA Analysis of variance

ASC Adipose derived stem cell

BC Breast cancer

BCA Bicinchoninic acid

BLAST Basic local alignment search tool

BPA Bisphenol A

BRCA Breast cancer (gene name)

CAF Cancer associated fibroblast

CCL5 C-C motif chemokine ligand 5

COL Collagen

DAPI 4′,6-diamidino-2-phenylindole

DCIS Ductal carcinoma in situ

DMSO Dimethyl sulfoxide

ECM Extracellular matrix

EDTA Ethylenediaminetetraacetic acid

EGFR Epidermal growth factor receptor

EMT Epithelial to mesenchymal transition

ER Estrogen receptor

ETP Endotrophin

FASP Filter aided sample preparation

FBS Fetal bovine serum

FDR False discovery rate

FITC Fluorescein isothiocyanate

GFM Gene coding for Elongation Factor G1; mitochondrial

GTA Glutaraldehyde

Gy Gray (SI unit of radiation)

HER2 Human epidermal growth factor receptor 2

IFG1 Insulin-like growth factor 1

IL-6 Interleukin 6

JNK c-June N terminal kinase

Ki67 Gene name, critical for ribosomal RNA synthesis. Name originates from Kiel, Germany, where it was discovered.

LD Latissimus dorsi

LIC Lobular *in situ* carcinoma

MMP Matrix metalloprotease

MMTV PyMT Mouse mammary tumor virus – Polyoma middle T.

MRPS12 Mitochondrial ribosomal protein S12

MSC Mesenchymal stem cell

mTOR mammalian target of rapamycin

NADH Nicotinamide adenine dinucleotide (H = reduced form).

NFkB Nuclear factor kappa-light-chain-enhancer of activated B cells

PABC Pregancy associated breast cancer

PARP Poly (ADP-ribose) polymerase

PBS Phosphate buffered saline

PR Progesterone receptor

RAD51 Family of DNA double stranded break repair genes

RIPA Radioimmunoprecipitation assay buffer

RPS21 Ribosomal protein S21

SHG Second harmonic generation

Src Proto-oncogene name in sarcoma development

SRP9 Signal recognition particle 9

TACS Tumor associated collagen signatures

TAM Tumor associated macrophages

TNBC Triple negative breast cancer

TRAM Transverse rectus abdominus muscle

Scientific papers resulting from this PhD thesis

Oncotarget. 2018 Jun 12;9(45):27895-27906.

Breast cancer recurrence after reconstruction: know thine enemy.

Brett EA[1], Aitzetmüller MM[1], Sauter MA[1], Huemer GM[2], Machens HG[1], Duscher D[1].

Breast Care (Basel). 2019 Oct;14(5):278-287.

Novel Assay Analyzing Tropism between Adipose-Derived Stem Cells and Breast Cancer Cells Reveals a Low Oncogenic Response.

Sauter MA[1], Brett E[1], Müller CM[1,2], Machens HG[1], Duscher D[1].

Journal of Clinical Medicine. 2020 Apr 2;9(4). pii: E991.

Oncogenic Linear Collagen VI of Invasive Breast Cancer Is Induced by CCL5.

Brett E[1], Sauter M[1], Timmins É[2], Azimzadeh O[3], Rosemann M[3], Merl-Pham J[4], Hauck SM[4], Nelson PJ[5], Becker KF[6], Schunn I[7], Lowery A[8], Kerin MJ[8], Atkinson M[3], Krüger A[9], Machens HG[1], Duscher D[1].

Accepted at Cancer and Metabolism, June 2020

Tumor associated collagen signatures: pushing tumor boundaries

Brett E, Sauter M, Machens HG, Duscher D

Introduction

The breast - organ

Breast tissue origin and overview

The human breast is a modified apocrine sweat gland, which sits on the chest wall between ribs number 2 and 6, anterior to the fascia of the pectoralis muscles. Although present in both males and females, the female mammary gland is highly developed and is essential as a reproductive organ (1). Origin of breast tissue occurs between week four and six of embryonic development, along the mammary ridge (‘milk line’), which extends from the axilla to the groin. Any extra (‘accessory’) mammary structures, e.g. breasts or nipples, are found along this line. The phase of building ducts and glands is called ‘branching morphogenesis’. This begins *in utero* at equal rates for both genders, is paused during childhood, and restarts in puberty under the correct hormonal environment, found predominantly in females (2). Pubertal hormonal balance is dependent on sufficient adipose tissue deposits in women. This is classically exhibited in female athletes/gymnasts who undergo delayed puberty due to maintenance of low body weight during pubertal development (3, 4).

Normal breast anatomy

The gross structure of the breast is a tear drop shape, beginning superiorly in the deep fascia of the axilla, and extending inferior and medial along the anterior chest wall. Internally, the breast has an arborized structure, with lobes of functional parenchyma called ‘alveoli’ separated by planes of soft tissue (5). These stromal septae partition the breast and follow a course anterior to the nipple-areola (mammilla) complex. Arising from the subclavian artery is the internal thoracic/mammary artery, and is the main blood supply for the breast (6). As the artery runs inferiorly, it bifurcates at the level of rib six/seven into the superior epigastric and musculophrenic arteries. Concordantly, the large internal thoracic vein and lymph nodes follow the same course as the artery (7).

Lymph nodes collect in the axilla and act as important sentinel check points in the diagnosing and staging of breast cancer (8).

Acinar structure

'Acinus' is the term given to a cluster of epithelial cells, as in sweat glands or alveoli in the lung (acinus is Latin for 'berry', plural acini) (9). The functional unit of the breast is the acinus, made of a drainage duct connected to a collection of luminal epithelial cells which have a baso-apical polarity axis. The secretory apical pole of the cells face a hollow lumen, and the basal pole is attached to a basement membrane, made chiefly of collagen IV and laminins, connected by the glycosaminoglycans perlecan and nidogen (10). The epithelial cells secrete milk and are bound to one another at the apical surface by tight junctions (zonula occludens) (11). Surrounding this spherical structure are myoepithelial cells, which serve to physically squeeze the acinus, pushing the milk product out through the acinar duct (12).

Pathology

Breast cancer

The breast tumor is the most common tumor worldwide (13). Diseases/pathologies of the breast tissue are wide ranging in structure and severity. Non-neoplastic, inflammatory, or proliferative diseases are considered benign, and generally managed conservatively, if at all (14, 15). For example, fibroadenomas, typically found in young women, are hard, round and well defined. In this case, the pathological structure does not anchor itself in surrounding tissue, and are so motile they are sometimes referred to as 'breast mice'. Fibroadenomas usually involute during menopause and do not progress from their benign state (16).

Epithelial hyperplasia is the increase in numbers of epithelial cells, with cells of the duct most commonly experiencing hyperplasia (the first steps in developing 'ductal carcinoma'). However, so long as the multiplying cells remain within basement

membrane of original structure, they are considered benign and not yet evolved to malignancy (17). Epithelial to mesenchymal transition (EMT) is a term used to describe cells transitioning in embryonic development, and also in cancer progression. Specifically, it is a morphologic change in the affected cells, featuring detectable characteristics like loss of E-cadherin, and increases in vimentin and N-cadherin (18). A wide array of carcinomas arise once EMT occurs. Malignant lesions include in situ carcinoma (ductal/lobular origin), invasive carcinoma, medullary carcinoma, and papillary carcinoma (19). Ductal carcinoma in situ (DCIS) is the phase before invasive carcinoma; '*in situ*' referring to the fact it has not broken through the basement membrane of the host lobule/acinus. Ductal invasive carcinoma (DIC) implies EMT has occurred, and the cancer has become malignant. Not only is DIC the most common, it also has the poorest prognosis. Lobular invasive carcinoma (LIC) is the second most common (10% of all breast cancer cases) (20).

DIC can lead to collagen deposition, 'desmoplasia', in the breast, making it difficult for radiographers to distinguish healthy tissue from cancer tissue (fibrotic tissue is referred to as 'hyperechoic' for its amplified signal) (21). These carcinomas are directly contrasted by the self-isolated fibroadenoma, in that the invasive tumors build extensively into the surrounding healthy parenchyma. The histological presentation of the cells at the border of the DIC/LIC tumor are in single file, along tracts of linear collagen. The rows of cells are organized in lines directed away from tumor into local parenchyma (22, 23).

This observation is critical, as it is the cellular manifestation of a much larger fibrotic process at play, discussed later on in 'Tumor associated collagen signatures'.

Triple negative breast cancer

Triple negative breast cancer cells lack receptors for three factors; progesterone (PR), estrogen (ER) and human epidermal growth factor (HER2) (24). The fast speed of growth and brain/lung metastatic targets of this cancer subtype makes it the most lethal form of breast cancer. Within the TNBC classification there are 4 different types; mesenchymal, luminal, basal-like 1 and basal-like 2 (25). TNBC expresses EGFR (26), and activates pathways involving mTOR (27) and Src (28). The lack of hormone

receptors on the cell membranes mean no classic hormonal treatment is applicable. The TNBC tumor presents itself as 'basal-like', meaning its pattern of expression is similar to normal basal epithelial cells (29). Histologically, the cells of the tumor are small, round, and mostly uniform. Importantly, the cells are commonly seen in a single-file format, leading away from the center of the tumor (30). Once again, this observation echoes throughout the literature and will be addressed in 'Tumor associated collagen signatures'.

Demographics and epidemiology

10-20% of breast cancer diagnoses are TNBC (31). Despite the frequency of TNBC, it is a heterogenous disease which makes consensus across large scale epidemiologic studies difficult. However, studies conducted in smaller cohorts share several main findings. In terms of population prevalence, TNBC is generally seen to develop in women under the age of 40 (32). There is also evidence for higher disease presence in women of color, specifically African-American women, and lowest disease presence in Filipino women (33). Genetically speaking, cancer cell receptor deletions resulting in TNBC are most likely to arise in carriers of the BRCA1 mutation (34). Similarly, TNBC in a first-degree family member significantly increases the chances of diagnosis (35). Prolonged breast-feeding serves as a protective physiologic event against TNBC (36). However, the buildup and tear down of breast anatomy opens up the tissue to oncogenic risk; specifically, women in the first 5 years post-partum (37). The mere act of breast stroma and parenchyma involution can lead to a rare event called pregnancy associated breast cancer (PABC). It affects 3 per 10000 births, but is so notable due to its low survival rate (38).

Risk factors

Multiple risk factors exist for developing TNBC. The highest risk is a mutation in the BRCA gene, commonly discovered through genetic counseling (39). BRCA codes for the protein BRCA1 which aids DNA double stranded break repair (40) by binding with RAD-51 at the site of DNA lesion (41). Such unrepaired damages lead to a variety of cancers, primarily of the breast. Another risk factor is women who do not have children.

Women who have children in the first 20 years of life are 50% less likely to develop TNBC compared to nulliparous women (42). Specifically, only full term pregnancies protect against breast cancer in later life; women who have aborted the pregnancy have no benefit against cancer development (43). The mechanism of this protection is not fully understood, but it is believed to be enhanced IGF1 signaling through the cocktail of hormones specific to pregnancy, which epigenetically alters the epithelial cells (44).

Another recently recognized and correlated factor is breast density. Not only does dense breast tissue obscure potential lesions from radiologists (45), but the desmoplastic environment alone is enough to stimulate cancer development (46).

Similarly, obesity puts women at risk for multiple diseases, including cardiac /pulmonary disease, musculoskeletal complications, and a range of cancers including breast cancer (47).

High circulating estrogen levels have also been linked to BC development. Estrogen has a profound proliferative effect on breast ductal epithelia (48). While endogenous estrogen has been linked epidemiologically and experimentally to BC (49), exogenous estrogen can be equally as effective in promoting BC growth. Bisphenol A (BPA), found in many plastics, which leaches out into food and drink products, enters the circulation where it acts as a xeno-estrogen, causing ductal density and further sensitivity to estrogen (50). High levels of circulating BPA have also been correlated with increased breast density (51).

Smoking significantly increases breast cancer risk. Specifically, breast epithelial cells acquire a fibroblastic morphology when exposed to cigarette smoke (52), via polycyclic hydrocarbons produced by burning. Polycyclic hydrocarbons act as bulky adducts to DNA. They bind and physically twist DNA to cause physical base pair mutations (53).

Therapeutic options

TNBC tumors are extremely intractable and difficult to treat. Given the high Ki67 expression of TNBC cells (54, 55), the best course of action currently is a rigorous regime of chemotherapy, coupled with surgery and radiation (56).

Surgical options are centered around ensuring an R0 resection. R0 is defined by a histological examination of margins left *in situ* by the surgeon, showing zero detectable

evidence of disease (57). For instance, a positive margin (described as R1) increases the risk of cancer recurrence from the minimal residual disease left in the body (58). Different pharmacological courses of treatment exist. One such option includes taking advantage of the DNA reparative Poly-ADP ribose polymerase (PARP) enzymes (59). It so follows that hindering the DNA repair process using PARP inhibitors along with administering cytotoxic agents can effectively damage the rapidly hyperplastic cancer cells to a lethal extent (60). Paclitaxel (Taxol) represents a gold standard for TNBC pharmacological treatment, and is frequently given in combination with Bevacizumab (Avastin) to TNBC patients (61). Together they act to destabilize mitotic microtubules and VEGF signaling, respectively (62).

Reconstructive surgical options

There are three surgical mainstays in breast reconstruction; flaps, expanders/implants, and fat grafting. Flaps are defined as transferred *en bloc* tissue resections from one location to another. Generally, they are blocks of tissue removed from the host site, including a length of the main supplier blood vessel. 'Free flaps' are removed completely from the donor site, by severing the tissue and main supplier vessel, and anastomosing it directly into recipient site circulation (e.g. radial forearm flap with radial artery, transverse rectus abdominus muscle flap (TRAM flap) with the deep inferior epigastric artery) (63). A 'pedicle flap' is raised from the donor site, but remains local, as the vessel is not severed. Rather, the tissue is moved to a local recipient site, preserving the vasculature (64). Similarly, and frequently in breast reconstruction, a latissimus dorsi flap (LD flap) is raised from the back and swung anteriorly to create a breast mass (65).

Another common method of creating breast masses involves implants and/or fat grafting. These options often necessitate the initial use of a tissue expander, loosening the skin of the chest wall for six - eight weeks (66). Fluid based tissue expanders placed under the skin exert positive pressure to create a space for implants/fat tissue, while suction cups placed on the chest wall uses negative pressure to draw skin away from the chest, also creating a space (e.g. BRAVA negative pressure system). The pocket created by suction has almost double the amount of neovascularization compared to

pockets created with positive pressure (67, 68). This is critical when considering what material will fill the newly created chest wall space.

Fat grafting is a procedure defined firstly by the suction of fat tissue, generally from the abdomen. The fat tissue is then centrifuged, so it may separate into layers (cell/large debris pellet in the bottom, blood and tumescent surgical fluid in the center, and broken down adipose tissue on top) (69). The adipose tissue is then transferred to a grafting device and injected wherever necessary (70), in this case, the breast. Fat grafting generally accompanies all forms of breast reconstruction, given its ease of completion and ability to correct minor volumetric flaws. However, with the grafting of fat, comes a new healthy cell population which surgeons are wary of introducing to a zone which once was cancer positive. The oncological fear of causing recurrence via fat grafting is well-described (71), and the *in vitro* testing of cancer cells and adipose derived stem cells has shown production of oncogenic cytokines (72-75). The publications with such findings actually warn the surgeon against fat grafting, citing the pro-oncogenic impact of adipose derived stem cells and cancer cells *in vitro*. However, these data are mainly based on the classic Boyden chamber insert. This assay leaves a lot to be improved if such a valuable surgical option is to be abandoned.

Tumor associated collagen signatures (TACS)

As discussed before, cells at TNBC tumor borders are frequently found in strings; a single-file format which point outwards from the core of the tumor. TNBC tumors are bordered by an invasive outer layer of linearized extracellular matrix (ECM) which grows outwards into the healthy breast (76). Striated collagen is oriented in a way to expand tumor growth and facilitate intravasation (3, 77, 78). However, the origin and construction of these organized collagen structures are completely unknown.

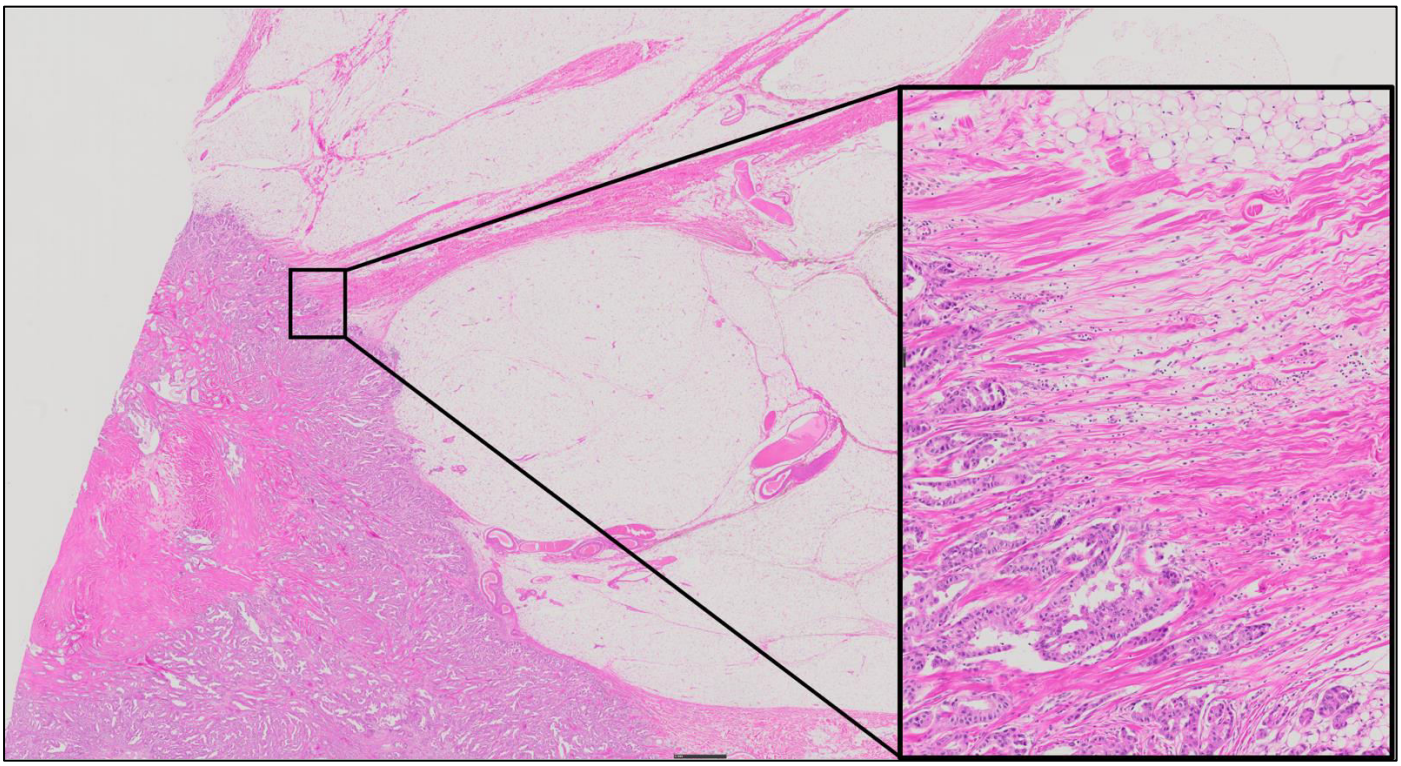

Figure 1: H&E stain of a triple negative invasive breast tumor, interfacing with healthy stroma. Zoomed panel show invasive tracts of collagen interspersed with cell nuclei. Scale bar 500μm University of Basel, *Pathorama.* (Used in accordance with guidelines; https://pathorama.ch/vslides/index.html).

The most cogent description of TNBC tumor collagen heterogeneity was first written in 2006. Provenzano *et al* created the term 'tumor associated collagen signatures' or TACS, to describe 3 distinctly different shells of the tumor, radiating outwards (76). The proposed system described TACS1 as an increased deposition of collagen directly around the tumor body. TACS2 is the middle layer, an arrangement of the collagen in onion-like layers, encasing the tumor. TACS3 is the outer zone, a system of coordinated perpendicular threads of collagen leading directly away from the tumor and into the surrounding tissue (**Figure 1**). The group used second harmonic generation microscopy (SHG) to visualize the TACS3 collagen pattern in intact, unfixed human mammary glands. SHG is a non-linear microscopy technique which gives sub-micron resolution of fibrillar collagen *in vivo*. It has previously been used to image uterine cervical tissue and the linearity of collagen therein (79).

A

Year	Title
2006	- **Collagen reorganization** at the tumor-stromal interface facilitates local invasion.
2011	- **Aligned Collagen** Is a Prognostic Signature for Survival in Human Breast Carcinoma
2014	- Automated quantification of **aligned collagen** for human breast carcinoma prognosis
2016	- Changes of **collagen ultrastructure** in breast cancer tissue determined by second-harmonic generation double Stokes-Mueller polarimetric microscopy. - **Oriented collagen** fibers direct tumor cell intravasation.
2017	- Quantifying **collagen fiber orientation** in breast cancer using quantitative phase imaging. - Identification of **prognostic collagen signatures** and potential therapeutic stromal targets in canine mammary gland carcinoma. - **Tumor-associated Collagen Signatures**: An Insight - Patient-derived Interstitial Fluids and Predisposition to Aggressive Sporadic Breast Cancer through **Collagen Remodeling** and Inactivation of p53.
2018	- Second-harmonic patterned polarization-analyzed reflection confocal microscopy of **stromal collagen** in benign and malignant breast tissues. - Targeted matrisome analysis identifies thrombospondin-2 and tenascin-C in **aligned collagen** stroma from invasive breast carcinoma. - **Biophysics** of Tumor Microenvironment and Cancer Metastasis - A Mini Review. - The Presence of Cyclooxygenase 2, Tumor-Associated Macrophages, and **Collagen Alignment as Prognostic Markers** for Invasive Breast Carcinoma Patients. - **Collagen Alignment** as a Predictor of Recurrence after Ductal Carcinoma In Situ.
2019	- Regulation of migration of chemotactic tumor cells by the spatial distribution of **collagen fiber orientation**. - The role of collagen in cancer: from bench to bedside - **Fiber alignment** drives changes in architectural and mechanical features in collagen matrices - Microextrusion printing cell laden networks of type I collagen **with patterned fiber alignment** and geometry

B

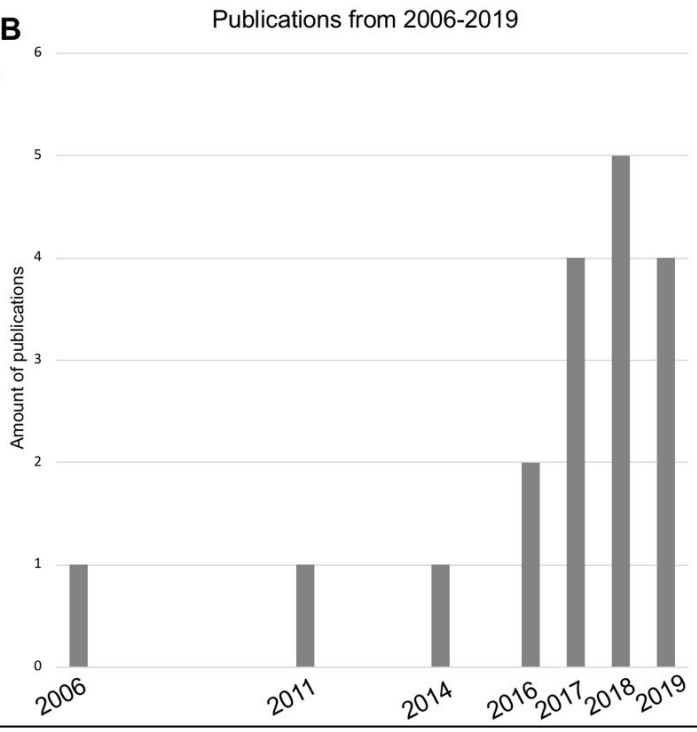

Figure 2: List and graph of publications featuring TACS. A) List of publications resulting from PubMed keyword search using 'linear collagen' AND 'breast cancer', 'tumor associated collagen signatures' AND 'breast', 'oriented collagen' AND 'metastatic'. B) Chronological graph showing upgoing trend of publications featuring the keywords in (A). References (76, 77, 80-95).

Two years later, the same group devised a novel *in vitro* assay in which tumor explants and/or MDA-MB-231 triple negative breast cancer cells were cultured at 2 distinct focal points in a collagen gel. The collagen in between these points changed layout within 10 days of culture, from a stochastic pattern to an organized linear arrangement. Along with increased cancer cell migration along these structures, it was ascertained that the collagen alignment is governed by the Rho/Rho kinase pathway (96) Interestingly, it was shown that higher collagen density is directly linked to higher cancer cell invasion. Using an MMTV-PyMT transgenic mouse model of spontaneous mammary carcinoma, higher levels of collagen were seen deposited around the tumor (TACS1 and TACS2) leading to increased local invasion and metastasis (97). Therefore, not only is breast density a known confounder of mammographies (98), but higher breast density itself may be a cause of cancer development. Research from 2018 showed that cells cultured in a less dense collagen gel led to oxidative phosphorylation in MDA-MB-231 and MDA-MB-468, and culture in a denser collagen gel led to increased levels of free NADH, a

product of glycolysis (99) (100). This study illustrates how collagen density can alter cancer cell metabolism.

The affirmation of the TACS3 concept and its clinical relevance was substantiated with a study of 196 human histopathology breast tumor biopsies. Image analysis of histological sections showed robust formation of TACS3 collagen structures, and samples with TACS3 were directly linked to worse patient prognoses (80). To provide more evidence of the viability of TACS as a model, a method to mathematically quantify TACS3 was developed. Presence of TACS3 was therein proposed as a structural biomarker for cancer severity, which is not yet a mainstay in clinical diagnoses (81).

Purpose of this study

This research project aimed to fill a knowledge gap of how linear collagen is deposited by triple negative breast cancer cells. Considering the fascinating decellularization research *in vitro* (101), and the feasibility of an *in vitro* matrix deposition model (102), experiments were designed to investigate the hypothesis: *CCL5 is required for successful linear collagen formation by cells of invasive breast cancer.*

Materials and Methods

Table 1: Reagents used for *in vitro* experiments

Reagent	Category number	Supplier
DMEM, high glucose, pyruvate	41966029	Gibco
Fetal bovine serum	16000044	Gibco
Penicillin Streptomycin	10378016	Gibco
Phosphate buffered saline	10010023	Gibco
0.025% Trypsin/EDTA	R001100	Gibco
StemMACS™ MSC Expansion media	130-104-182	MACS Miltenyi Biotech
MitoTracker™ CMX-Ros	M7512	Thermo Fisher Scientific
MitoTracker™ Green FM	M7514	Thermo Fisher Scientific

Cell lines

TNBC cells (MDA-MB-231, ATCC® HTB-26™), Human fibroblasts (HS-27, Sigma Aldrich cat# 94041901-1VL), adipose derived stem cells (ASC) (Poietics™, donors 29635, 31363, cat# LO PT-5006) were all purchased and used in the downstream experiments. Cell stocks were created in the early stages of culture to maintain passage <15. Cells at passage 15 were discarded and replaced with thawed stocks.

Cell culture

Normal culture conditions included a humidified chamber at 37°C with 5% CO_2. All cell culture work in this project was carried out at these parameters. MDA-MB-231 and fibroblasts (HS-27) were cultured in DMEM (Dulbecco's modified Eagle's medium), 10% fetal bovine serum, and 1% PenStrep (henceforth referred to as ‘full media’). ASCs were specifically cultured in StemMACS rather than DMEM, with 10% FBS and 1% PenStrep.

Cell passaging and counting

Passaging of cells was performed by an initial wash of the cells with 1X PBS (Gibco), and subsequent incubation of 0.25% Trypsin/EDTA with a volume appropriate for the surface area of cell culture dish used. Enzymatic incubation lasted for 5 minutes in a 37°C humidified incubator. Full media was then added to the trypsin/EDTA at double the

trypsin/EDTA volume, transferred to a volumetric tube and centrifuged at 1200xg for five minutes to obtain a pellet of cells. Supernatent was poured off and pellet was resuspended according to approximate size and cell number present. Counting was performed by transferring 10μL of suspension onto a Neubauer haemocytometer. The solution was spread evenly over the counting grid by the haemocytometer coverslip (103). All 4 grids were counted, added, and divided by 4 so to calculate the average. Cell number was determined by the following calculation:

$$Average\ cell\ count\ per\ grid\ \times\ 10{,}000\ \times\ volume\ of\ suspension\ (ml) = total\ cell\ yield$$

Cryopreservation and cell thawing

Cryopreservation was carried out on 900μL volumes of cell suspensions using dimethyl sulfoxide (DMSO). Specifically, 100μL of DMSO was assed to 900μL of cell suspension, to achieve a 10% DMSO concentration in the cryovial (Thermo Fischer). Cells were frozen slowly using an ice box designed for -80°C storage containing isopropanol. Liquid nitrogen storage was used for longer term stocks. Cell thawing was done rapidly, by holding the frozen cryovial in a waterbath of 37°C, and quickly adding the melted contents to 10ml of full media. The solution was spun down at 1200xg for 5 minutes to obtain a pellet. Cells were then ready for expansion culture.

Cell staining

Prior to co-culture set up, MDA-MB-231 cells were stained with Mitotracker CMX-Ros and HS-27 and ASCs were stained with Mitotracker Red Green FM according to manufacturer's protocol. Briefly, stock was dissolved in DMSO in a 1mM concentration. The stock solution was added to the culture media 1:2000 (red) and 1:10000 (green) to an end concentration of 500nM. Cells were afterward incubated for 4h, then washed and prepared for *in vitro* co-culture arrangement.

Table 2: Plasticware used routinely for *in vitro* experiments

Item	Category number	Supplier
Falcon® 75cm^2 flask	353024	Corning
Falcon® 15cm^2 flask	353009	Corning
Falcon® 15 ml tube	352096	Fisher Scientific
Falcon® 50 ml tube	352070	Fisher Scientific
Boyden chamber inserts (6 well plate) 0.4μm pore	CLS3413-48EA	Merck
Boyden chamber inserts (24 well plate) 0.4μm pore	CLS3396-2EA	Merck
Boyden chamber inserts (6 well plate) 8μm pore	3428	Corning
Pipetman Diamond tips (10, 200, 1200μL)	F161630, F161930, F161110	Gilson
2-well culture insert	81176	Ibidi
Cell culture multiwell plate (six well plate)	657160	Greiner Bio-One
Cell culture multiwell plate (24 well plate)	662102	Greiner Bio-One
Parafilm®	P7793-1EA	Merck

Co-culture arrangement – ASC/MDA-MB-231 migration

Boyden chamber experiment: this was set up as normal protocol details: 50,000 ASCs were seeded in a Boyden chamber insert of a six well plate, which contained pores of 8μm. Below, 50,000 MDA-MB-231 were seeded, allowing paracrine contact between cell types. Media was replaced after 24 hours, and sampled for cytokine screening at 48 hours.

Novel migration assay: Per the experimental set up (Figure 3), two chambers were set up in one well of a six well plate, one insert in each half. In each chamber was seeded either ASCs or MDA-MB-231, so each well contained two cell types. 24 hours after seeding, the chamber surrounding the seeded population of ASCs was removed, while the chamber surrounding the MDA-MB-231 was left in place. The well was filled with 3.5ml media. The excess of media meant an overflow into the chamber containing the MDA-MB-231, allowing a paracrine connection between cell types.

The varying breast cancer (BC) cell numbers (1K, 10K, 100K BC) stands for the titration study which was run, to assess if more MDA-MB-231 cells stimulated more migration of ASCs.

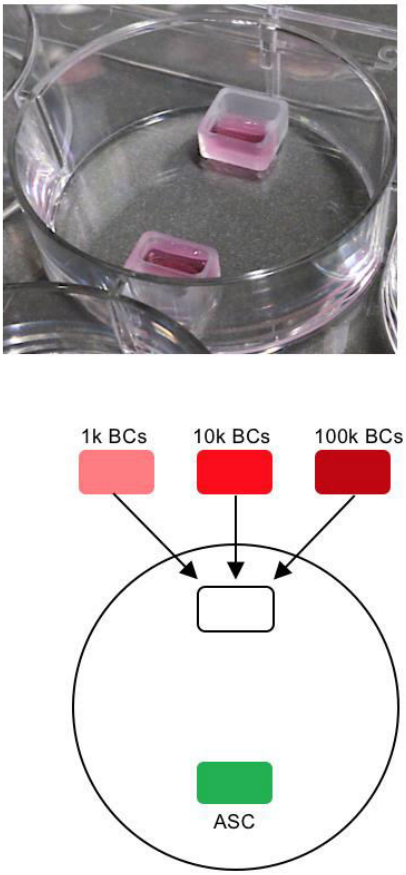

Figure 3: Schematic of novel *in vitro* migration assay. Top: gross image of six well plate containing two Ibidi inserts, each containing 70ul of media. Bottom: schematic showing division of cells, and a representation of how many MDA-MB-231 cells were seeded (1000, 10,000, or 100,000).

Co-culture arrangement – matrix deposition

An initial screening of 5 co-cultures was arranged, detailed in **Figure 4**. After observing initial findings, the groups were refined to three main types, detailed in **Figure 5**. Per 9.6cm^2, the surface area of one well of a six well plate, there were 50,000 total cells. All experiments were carried out in six well plates.

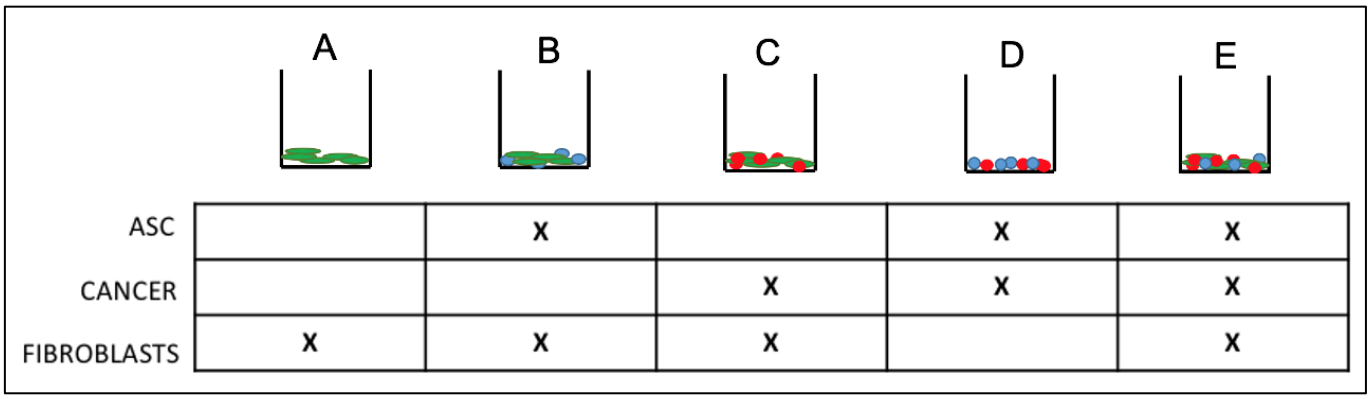

Figure 4: Schematic of initial screen of matrix deposition groups, containing cocultures per the table below. These groups were cultured and decellularized per the work flow in figure X.

Group i contained three cell types, added in equal quantity (16,666 cells per cell type).

Group ii contained 25,000 ASCs and 25,000 HS-27 cells. The Boyden chamber (0.4μm pore) was seeded with 20,000 MDA-MB-231.

Group iii had 25,000 ASCs and 25,000 HS-27 cells.

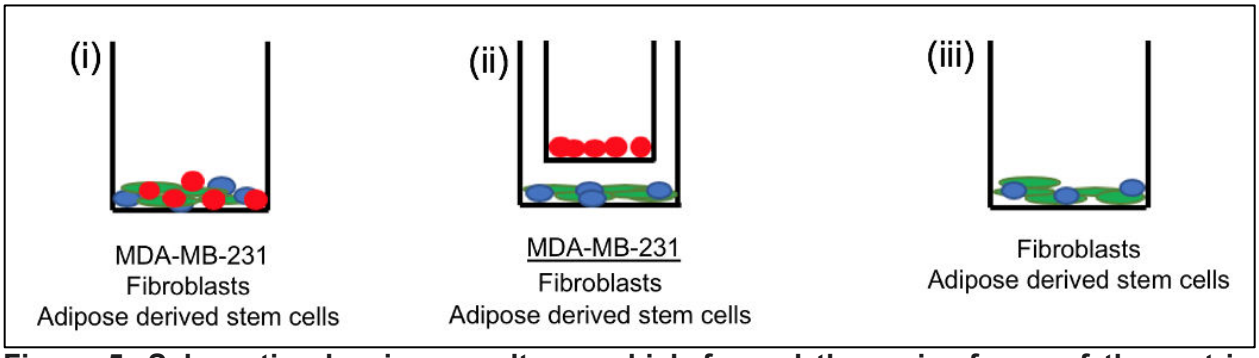

Figure 5: Schematic showing cocultures which formed the major focus of the matrix deposition experiments. Group i contained the three cell types of this study cultured together in a juxtacrine manner. Group ii also contained the three cell types, but the MDA-MB-231 cells were separated in a Boyden chamber allowing only paracrine contact. Group iii was the cancer-free culture, containing fibroblasts and ASCs cultured together in juxtacrine.

Matrix deposition and decellularization

Table 3: Reagents used for decellularization experiments

Reagent	Category number	Supplier	Experimental concentration
Gelatin from bovine skin type B	G6650-100g	Sigma Aldrich	0.5% in distilled water, sterile filtered
Glutaraldehyde	340855-25ml	Merck	2%, sterile filtered,

solution			stored at 4C
Ammonium hydroxide	338818	Sigma Aldrich	**Decellularization solution:** 20mM NH_4OH/1% Triton-X solution, sterile filtered, stored at 4C
Triton™ X-100	X100-100ml	Sigma Aldrich	
L-ascorbic acid	A8960	Merck	50mM solution prepared in distilled water, stored at -20C in aluminum foil to avoid photodegradation
Storage solution (Penicillin Streptomycin + Phosphate buffered saline)	10010023	Gibco	PBS containing 1% penicillin/streptomycin (PenStrep), stored at 4C

Preparation of plates

All plates to be used in matrix deposition experiments were initially coated with gelatin; involving a 2 hour incubation period containing the prepared gelatin solution at 37C. Plates were then removed from the incubator, gelatin was aspirated, and plates were fixed immediately with GTA. After fixation of five minutes at room temperature, plates were washed twice with PBS, and once with media. The purpose of the media wash was to allow the amines in the FBS to quench any remaining aldehydes. Plates were then ready for seeding and experimentation.

Culture period

Groups were cultured for seven days in total, before decellularization. During the week, culture media was prepared so cells received 50mM ascorbic acid days two, five, and seven. Cell layers were washed 2 x PBS on the eighth day of culture, followed by decellularization. This was performed by slow addition of warmed decellularization solution per **Table 3** (1ml/9.6cm^2), and incubation at 37°C for four minutes. Afterwards, decellularization solution remained in the plate, and PBS/1% PenStrep was added to the decellularized wells (at 2x the volume of decellularization solution). Plates were wrapped in Parafilm and stored at 4°C, for up to 5 days without fixation. Before

experimentation, all decellularized matrices were washed 3 x PBS.

Blocking experiments

In all experiments blocking CCL5, a monoclonal antibody (anti-human CCL5) was used (kindly supplied by Professor Nelson, LMU). Experiments featuring added CCL5 were run using purchased recombinant protein (CCL5) (Peprotech, cat# 300-06). Final experimental culture concentration for both the antibody and recombinant protein was $10\mu g.ml^{-1}$.

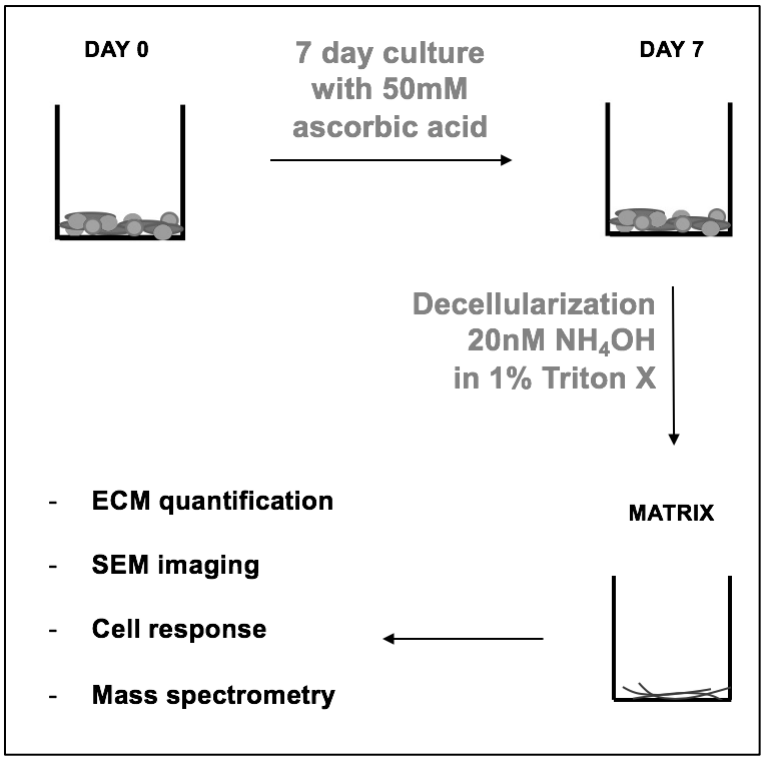

Figure 6: Schematic showing matrix deposition workflow. Total time from seeding to decellularization is eight days. Diagram runs clockwise to show 4 experimental options with decellularized matrix.

Table 4: Kits used commonly for in vitro experiments

Kit	Category number	Supplier
Pierce™ BCA Protein Quantification Kit	23225	Thermo Fisher Scientific
RNeasy Mini Kit	74104	Qiagen
One Step RT-PCR Kit	210210	Qiagen
TRIzol	15596026	Thermo Fisher Scientific
Human Cytokine Array C5	AAH-CYT-5-2	RayBiotech
Rabbit anti-human collagen VI antibody	AHP2049	BioRad
Goat anti-rabbit Alexa Fluor®488	Ab15077	Abcam
Mouse anti-human CCL5/RANTES	526402	Biolegend
Goat anti-mouse Alexa Fluor®647	Ab150115	Abcam

ECM quantification

After a 3 x PBS, solubilized matrices were quantified using a Pierce™ BCA Protein Assay Kit (#SA244529) per the protocol from manufacturer.

Cytokine array

On day five of the culture, 333μl of media was taken from each of the 3 replicates. The pooled 1ml of supernatent was tested per manufacturer's protocol using a Human Cytokine Array C5 (RayBiotech). Chemiluminescence was imaged after one minute of exposure on a ChemiDoc Imaging System (Bio-Rad).

Atomic force microscopy (AFM)

Glass coverslips were prepared for cell culture so as to have ECM samples which were not fixed to the six well plate. Cells were cultured and ECM decellularized as normal. Then, coverslips were thoroughly washed with PBS, and air-dried for 48 hours. ECM samples were removed from the well plate and were measured by POINTPROBE PLUS® silicon tips (resistivity 0.01-0.02Ω, PPP-NCHR-10) on a Dimension ™ 3100 Atomic Force Microscope (Digital Instruments).

Scanning electron microscopy (SEM)

As with samples for AFM, samples for SEM were also prepared on removable glass slides so as to accommodate the vacuum chamber of the SEM. As described, week-old co-cultures were decellularized, then fixed in 3.5% formaldehyde. Dehydration was performed with increasing alcohol concentrations (40, 60, 70, 80, 90, 95, 100%). Coverslips were air-dried in their original six well plate overnight, followed by gold sputter coating and imaging (Jeol JSM-6390 scanning electron microscope).

Immunohistochemistry (IHC)

IHC was performed on freshly decellularized matrices, within their original six well culture plate. Staining protocol involved blocking samples for non-specific binding with 10% serum (goat/rabbit, dependent on primary antibody). After a series of washes, the primary antibody was incubated in 1% blocking solution overnight at 4°C. The following day, samples were washed 3 x PBS and incubated with the secondary antibody at room temperature for one hour. After a 3 x PBS wash, 200µl DAPI/10% glycerol was added to the six well plate, and a coverslip was laid carefully on top to avoid air bubbles. Images were taken in a darkened microscopy room with a Zeiss Observer Z.1 AX10. Image analysis was performed using ImageJ (NIH).

Cell reseeding and imaging

Freshly decellularized matrices were washes 2 x PBS and 1 x fully supplemented media. Each 9.6cm^2 well received 2ml fully supplemented media, and was seeded with 20,000 MDA-MB-231 cells. Before incubation, plates were moved carefully on the surface of the laminar flow cabinet in a '+' shape, to allow for full coverage of the matrix by the cells, and to avoid a collection of cells in the middle. Plates were then cultured as normal and observed daily per brightfield microscopy.

Cell/matrix preparation for mass spectrometry

From the three experimental groups i, ii, and iii, only i and iii were selected for mass spectrometric analysis. As per established work flow, matrices derived from both groups were prepared over the week long experimental phase, reseeded with 10,000 MDA-MB-

231 cells, and cultured for 24 hours. Afterwards, the cell/matrix cultures were homogenized in RIPA buffer and protease inhibitor. Samples were kept on ice until filter aided sample preparation (FASP) on the same day.

Mass spectrometry and proteomic analysis

FASP digest was run on samples of 10µg cell/matrix extracts per existing standard protocol (104). Progenesis QI for proteomics analysis provided quantitative protein readout (105). Molecular signaling was interpreted via gene ontology term analysis with Ingenuity Pathway Analysis (IPA, Qiagen) (QIAGEInc.,https://www.qiagenbioinformatics.com/products/ingenuity-pathway-analysis) (106). Functional pathway analysis was run using STRING 11 (http://string-db.org) (107).

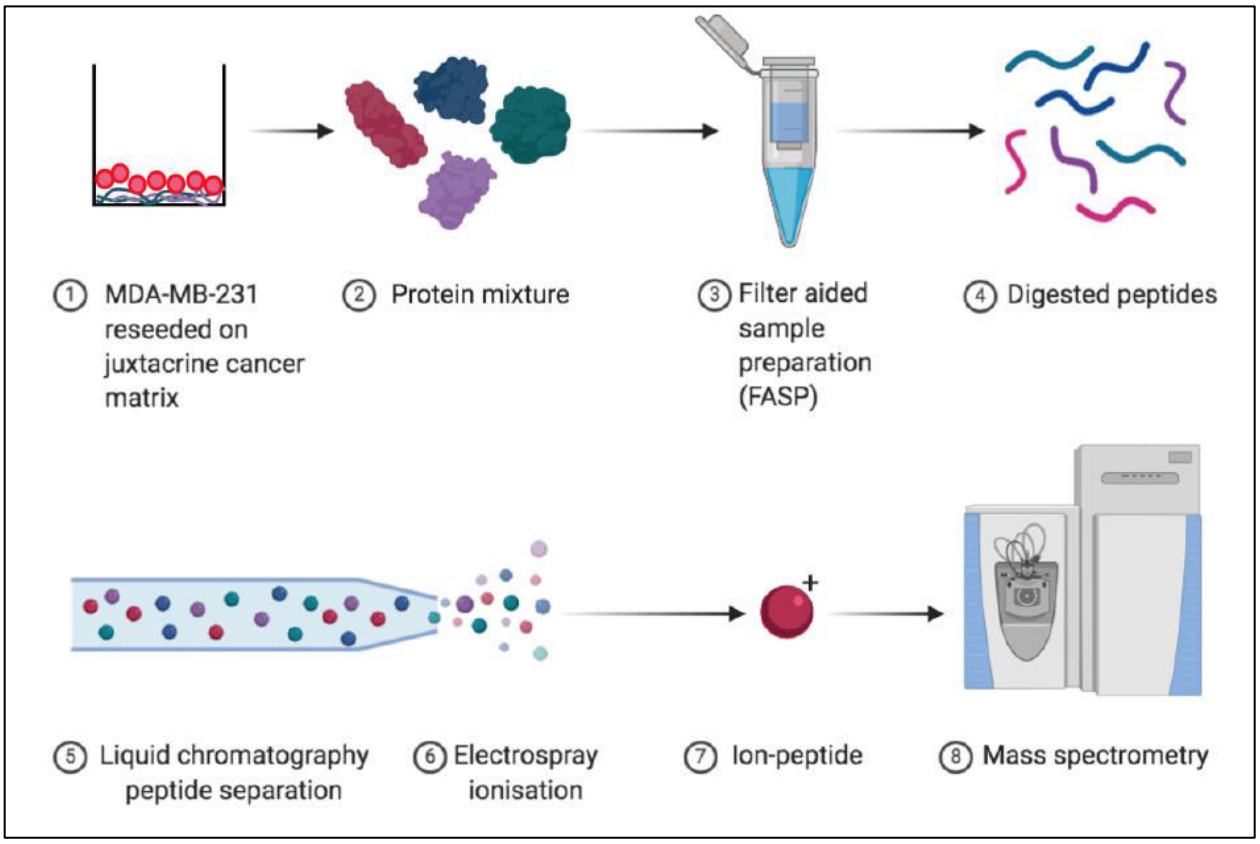

Figure 7: Workflow showing steps of protein generation and harvest for mass spectrometry. Generated partially with Biorender.

Polymerase chain reaction (PCR)

Cellular RNA was extracted using TRIzol™ (Thermo Fischer Scientific), and either stored at -80°C or processed that day. RNeasy Minikit (Qiagen) was used to isolate the genomic material from cellular/matrix debris. Downstream reverse transcription and PCR were performed using OneStep RT-PCR Kit (Qiagen). Primer design was confirmed by checking across Harvard Primer Bank (https://pga.mgh.harvard.edu/primerbank/), NCBI Gene (https://www.ncbi.nlm.nih.gov/gene/) and NIH BLAST tool (https://blast.ncbi.nlm.nih.gov/Blast.cgi). Primers for CCL5, SLUG, IL-6 and MMP3 were ordered from Invitrogen

CCL5 (Forward: GTGGCAGGCAGTAAGATAAACTTG, reverse: CAAAAAGCTTCCCCAACTAAAGC).

SLUG (Forward: CGAACTGGACACACATACAGTG, reverse CTGAGGATCTCTGGTTGTGGT

IL-6 (forward: ACTCACCTCTTCAGAACGAATTG, reverse: CCATCTTTGGAAGGTTCAGGTTG

MMP3 (forward: CTGGACTCCGACACTCTGGA reverse: CAGGAAAGGTTCTGAAGTGACC)

Histology of human samples

Three female patients underwent TNBC tumor removal, and consented for samples to be stored and analyzed (Technical University of Munich guidelines, ethics vote #2997/10). Three samples each from three patients were kindly given by the Department of Pathology at the TUM, specifically featuring the tumor border. Samples were paraffin embedded, and sections were cut at 70μm. H&E staining was carried out per existing protocols (108), and coverslips were mounted with Permount™ (Thermo Fischer Scientific).

Irradiation of cells

In order to assess ECM deposition by irradiated cells, cells were seeded in six well

plates as described in **Figure 6**, and cultured for one day to ensure attachment. Plates were then irradiated with one dose of 5Gy in a warmed chamber, and afterwards cultured per the normal protocol of 7 days. Viability assays were run 24 hours after irradiation. Matrices were prepared and decellularized as normal for downstream experiments.

Image analysis

For all cellular images, ImageJ was used to normalize brightness, calculate scale bars, compile fluorescent signals, and quantify pixel densiometry. Atomic force microscopy images were analyzed using Gwyddion software. Roughness of matrix surface area was quantified using the 'Roughness Calculation' plugin designed for ImageJ (2002).

Statistical Analysis

GraphPad Prism software was used to run all statistical analyses herein (GraphPad Software Inc., La Jolla, CA). Two groups were compared directly via two-tailed T-tests, and groups of three or more were analyzed using ANOVA (analysis of variance). Significance of *P* value had an upper threshold of 0.05, and error bars on all following graphs represent standard deviation from the mean.

Results

Novel migration assay shows a lower oncogenic response than conventional Boyden chamber experiment

The goal of this experiment was to devise a novel method of measuring the cytokines involved in ASC migration towards a fixed population of MDA-MB-231. This has normally been done using a Boyden chamber containing ASCs on a culture membrane with 8μm pores, with MDA-MB-231 cultured underneath. The results in the literature consistently show a pro-oncogenic response, however this does not match the clinical data which show clearly no cancer relapse when ASCs are introduced into a post-cancerous area (as in fat grafting). This novel experiment was designed to offer a different look at the same mechanism. The resultant data are more congruent with clinical outcomes.

Novel assay showed tropism in the direction of seeded MDA-MB-231 population over 24 hours

24 hours after removal of the chamber surrounding the ASCs, there was migration observed in the direction of the seeded MDA-MB-231, trapped in their insert, via paracrine communication. This was initial proof of concept that the ASCs had freedom to move, and did so in a directional manner (**Figure 8**).

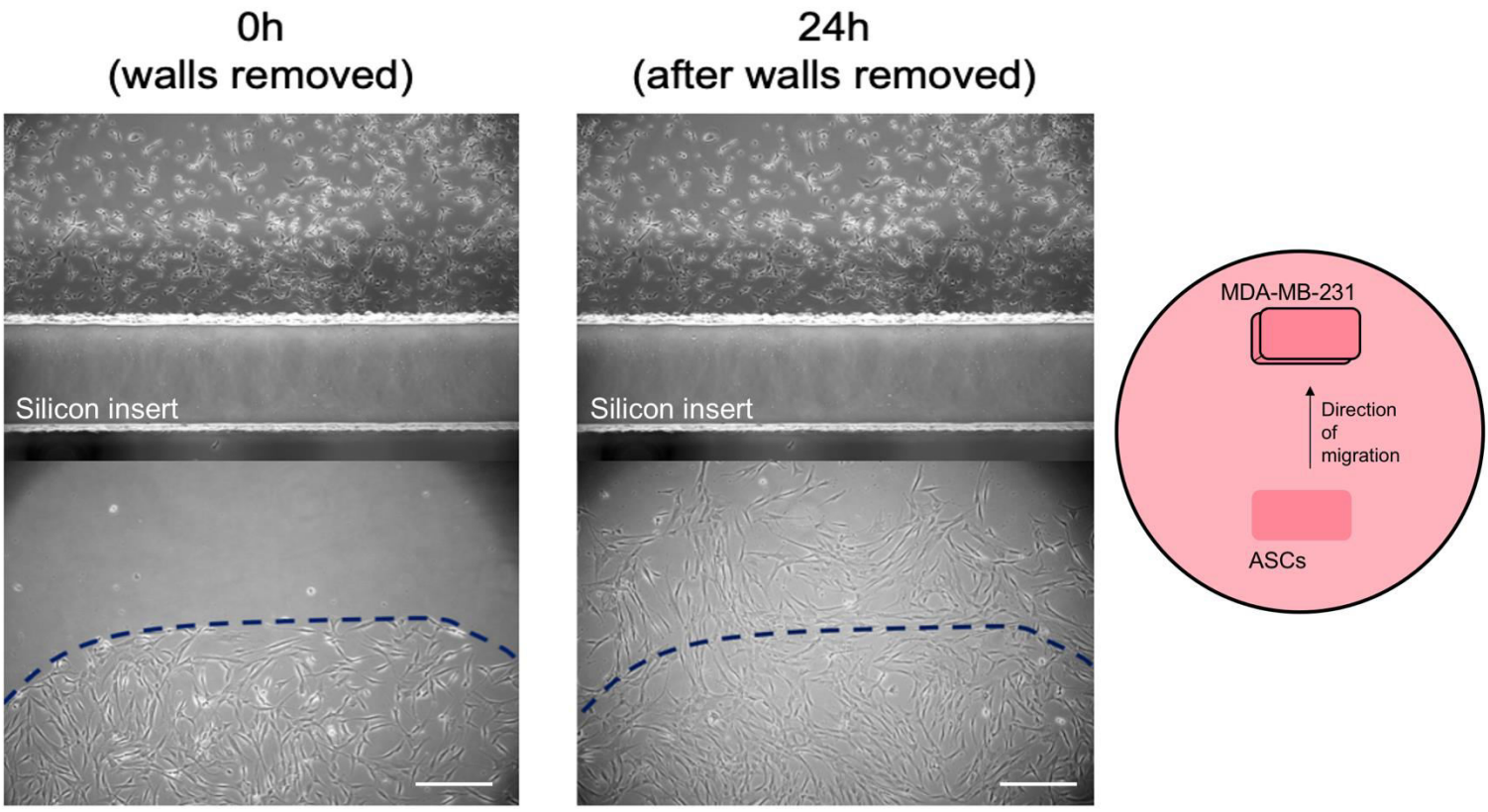

Figure 8: Directional migration of ASCs towards MDA-MB-231. Micrographs showing ASCs (bottom panels) and MDA-MB-231 within the silicon inserts (top panels). Bottom panels show at 24 hours a migration to the MDA-MB-231 cells located above. Schematic of cell positioning on the right hand side. Scale bar is 50μm.

IL-6 and CCL2 are highly upregulated in the Boyden chamber media compared to novel assay

Cytokine arrays were used to test the media from a pooled collective of n=3 per sample. Notably, 2 pro-oncogenic cytokines were seen to be highly upregulated in the media from the Boyden chamber assay, compared to the novel assay. It was only CCL2 and IL-6 which were upregulated; mirroring to the pro-oncogenic response normally recorded in the literature. However, the novel assay had the same cell numbers, culture time, paracrine contact, and media conditioning time, and did not show the same upregulation (**Figure 9**).

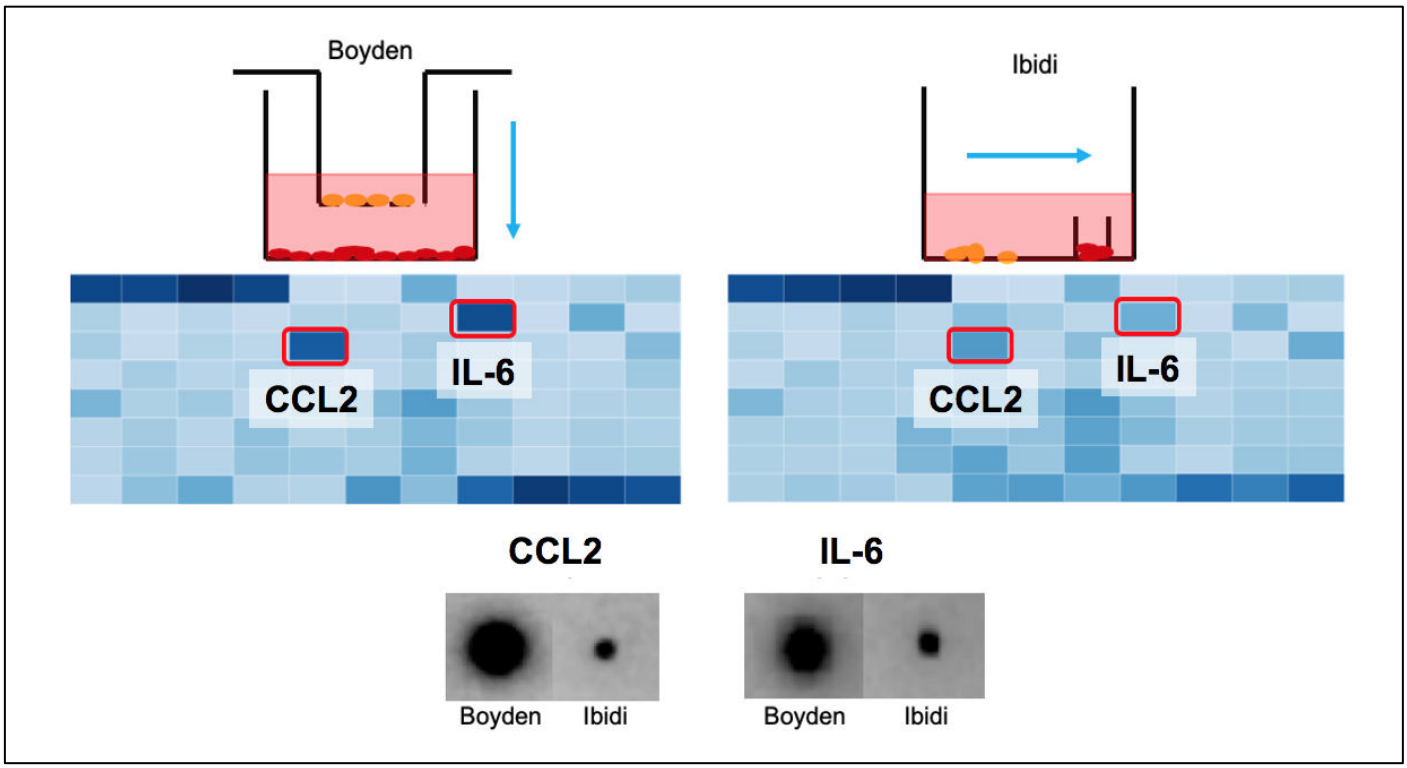

Figure 9: Less oncogenic cytokine profile belongs to novel migration assay compared to Boyden chamber assay. Top: schematics of both assay types. Left hand side is conventional Boyden chamber, right hand side is novel assay, after insert for ASCs (yellow) has been removed. Insert is surrounding MDA-MB-231 cells (red). Arrows show direction of travel. Middle: digitalized blot of 80 different growth factors/cytokines. Red outlines the two different cytokines between both assays. Below is the extracted blot from each different cytokine.

Seven days of culture gives quantifiable matrix

These experiments were run to assess the viability of *in vitro* matrix deposition, as a first step to designing the *in vitro* downstream experiments.

Matrices of different groups give different quantifications

From the multiple permutations of groups which were arranged (**Figures 4 and 10**), this screen test showed only one coculture which deposited smooth, linear matrix. The trio of cell types (MDA-MB-231, ASCs and fibroblasts) cultured together in juxtacrine contact and decellularized, produced flat matrix per SEM. When MDA-MB-231 cells were reseeded, they collectively formed unique, road like patterns (in red box) (**Figure**

10A). While this matrix was significantly less than other groups cultured (**Figure 10B**), the ultimate result from this experiment was the selection of the triple co-culture for further testing.

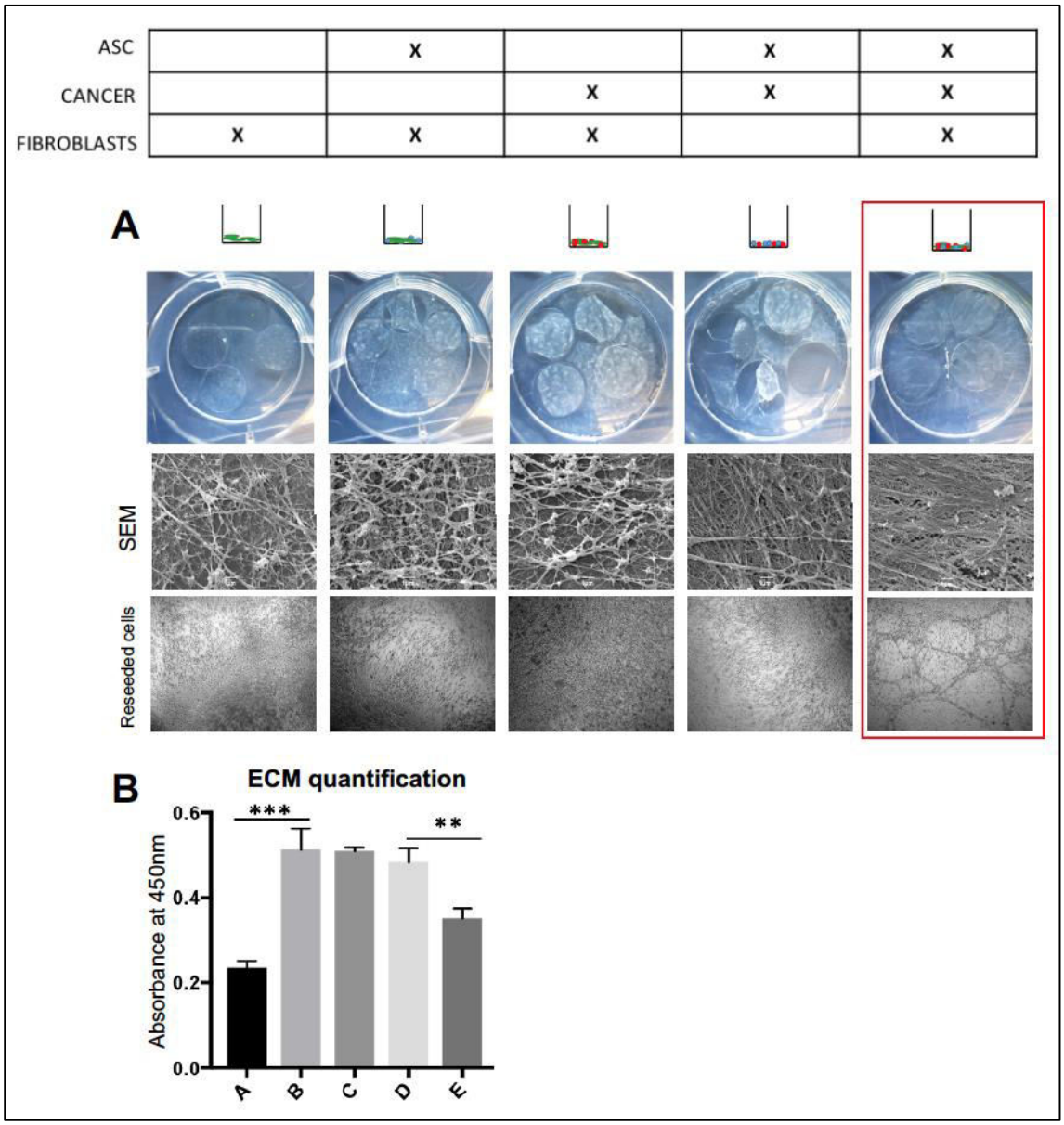

Figure 10: Smooth ECM is derived only in co-culture of ASCs, MDA-MB-231, and fibroblasts in juxtacrine contact. A) Table (above) and image grid (below) represent the permutations of cell combinations trialed in the preliminary work for obtaining linear matrix. Image grid contains images from gross microscopy (top row), SEM or decellularized matrix (middle row), and brightfield microscopy of reseeded cells (bottom row). Red box around group on the far right hand side represents the only combination of cell types that deposited a linear matrix, and which induced road-like structures in the reseeded MDA-MB-231 cells. B) Graph shows results of ECM quantification analyses. Significant differences represented by $^{**}p < 0.005$, $^{***}p < 0.001$.

Matrix deposited by MDA-MB-231 cells is insufficient for measurement or experimentation

It was discovered during the multiple test runs of ECM deposition co-culture groups, that the culture of MDA-MB-231 cells in a paracrine culture with either fibroblasts or ASCs did not deposit quantifiable matrix, per SEM (top images) (**Figure 11**). Similarly, when MDA-MB-231 cells were reseeded, there was no notable response, rather a normal monolayer of growth (bottom images).

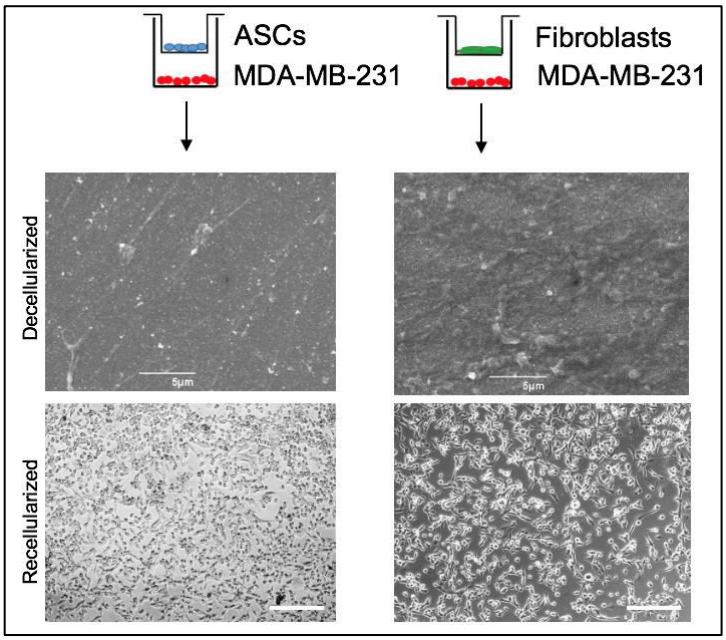

Figure 11: Matrix deposited by MDA-MB-231 is insufficient in quantity for testing. Top: schematic of cell groups seeded (MDA-MB-231 under paracrine influence of ASCs (left, blue) and fibroblasts (right, green). SEM images of decellularized matrix deposited (middle images) Reseeded cells on matrices shown in bottom images. Scale bar 50µm.

Matrices of different groups have different morphologies

Matrix deposition experiments evolved from the selection in **Figure 10** to three groups, henceforth referred to as groups i, ii,and iii. These three groups are further detailed in **Figure 12** below, and when cultured through the 8 day period and decellularized, produced high levels of matrix. Moreover, the matrices across each of the three groups differed greatly in morphology, as was visible to the naked eye (**Figure 12A**).

ECM generated by group i (ASCs, fibroblasts, and MDA-MB-231 cells together in juxtacrine) was smooth and striated.

ECM generated by group ii (ASCs and fibroblasts under paracrine influence of MDA-MB-231) was not abundant, and showed disorganized fibril deposition.

ECM generated by group iii (ASCs and fibroblasts) was thick, meshwork, and rich.

These results were visualized and confirmed with both SEM and AFM, as a first qualitative pass at characterizing the different matrices.

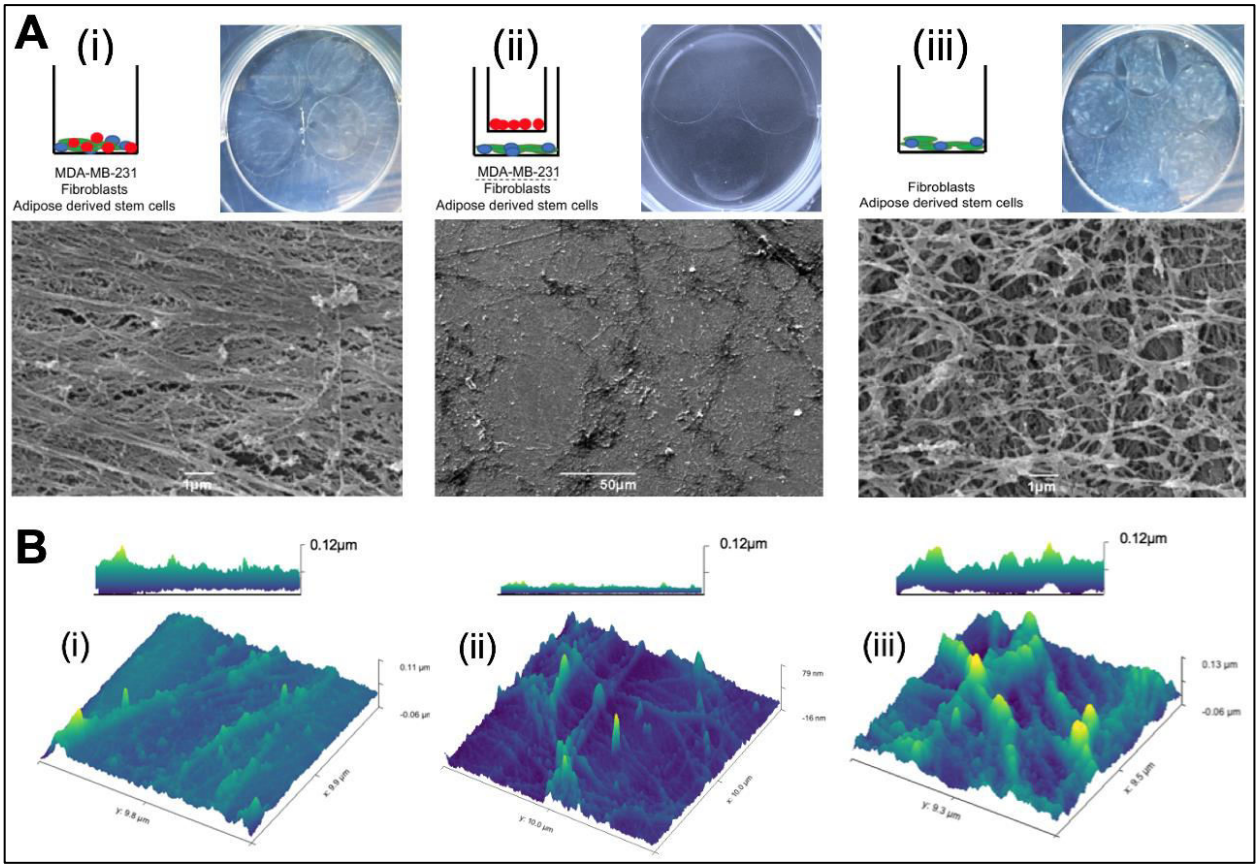

Figure 12: Three co-culture arrangements deposit three differing ECMs. A) Decellularized ECM on coverslips within the six well plate, accompanying schematics, and SEM. B) Three dimensional graphs from AFM show decellularized layers from groups i, ii, and iii. Maximum height of group i matrix = 0.11µm, maximum height for group ii = 80nm, maximum height for group iii = 0.13µm.

Matrices of different groups have different quantities

Quantification of protein from BCA assay showed group ii produced significantly less ECM than groups i and iii (**Figure 13C**). Matrix roughness quantification illustrates how matrix from group i (ASCs, fibroblasts, and MDA-MB-231) was the flattest, while matrix derived from group iii (ASCs, fibroblasts) was over twice as rough, with a significance level of $^{**}p = 0.008$ (**Figure 13D**).

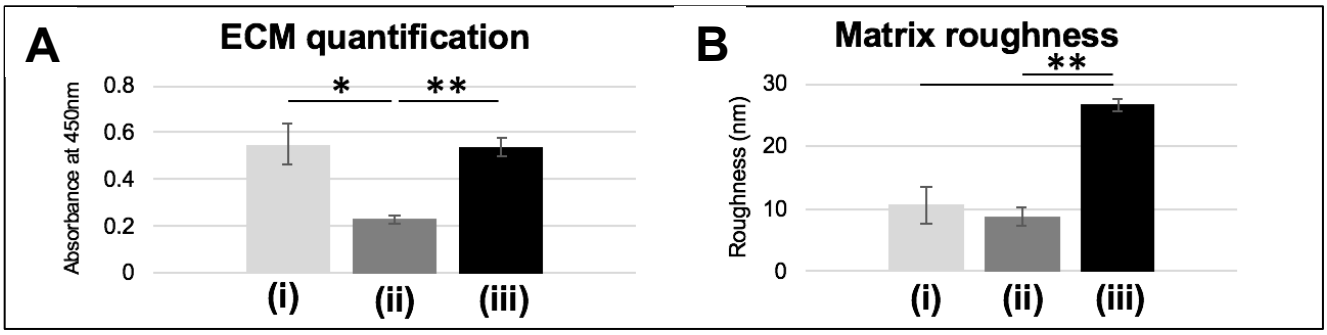

Figure 13: ECM quantification and roughness analysis between three co-cultures. A) Graph illustrates quantification of decellularized ECM per group. Standard deviation represented by error bars ($^{*}p$ <0.05, $^{**}p$ < 0.01). B) Graph illustrates roughness of decellularized matrix from values calculated by ImageJ. Standard deviation represented by error bars ($^{**}p$ < 0.01).

Important finding: ECM deposited by group i (ASCs, MDA-MB-231, and fibroblasts cultured side by side) was smooth, flat, with linear striations.

Matrix from healthy and cancer juxtacrine matrices have different proteomic make up

Mass spectrometry was run to assess the protein composition of the smooth cancer-derived ECM (group i) compared to the rough healthy ECM (group iii). The samples analyzed included the decellularized matrices with the MDA-MB-231 cells which were reseeded on them.

Cancer matrix has higher proportion of COL6A3

Mass spectrometry and subsequent proteomic analysis was performed on reseeded cell/matrix lysates from groups i and iii. A scan of extracellular matrix proteins revealed

a significantly higher amount of collagen VIα3 was present in group i compared to group iii (yellow data point in volcano plot of **Figure 14**) present in group i compared to group iii.

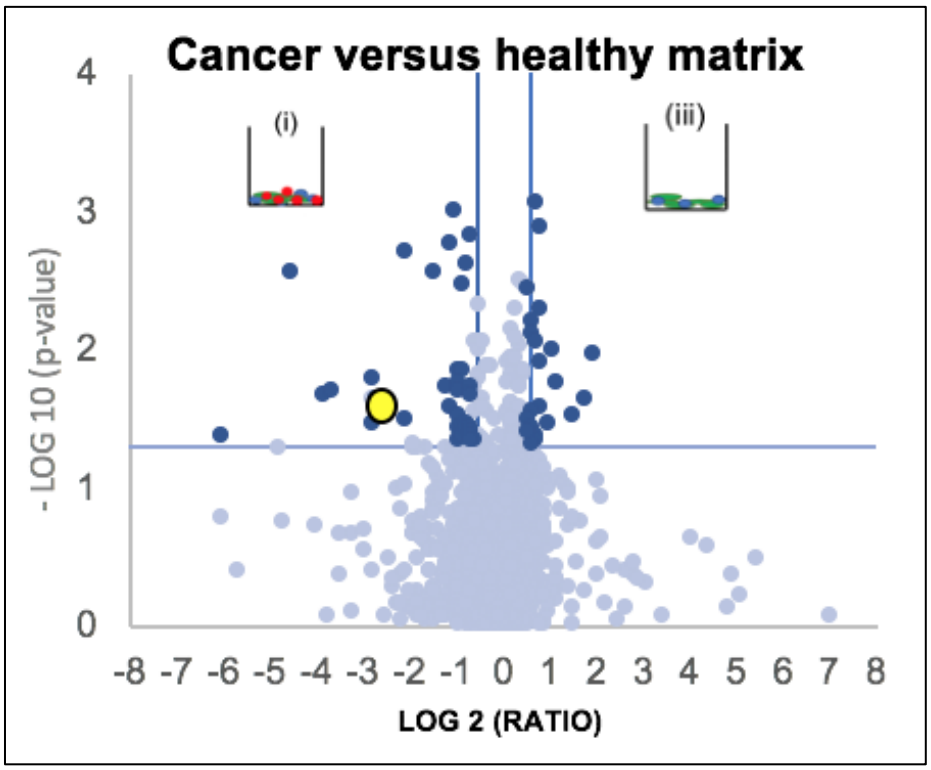

Figure 14: Volcano plot illustrating differences in proteome between group i and group iii matrices combined with reseeded cells. Yellow datapoint lying above the horizontal line of significance represents COL6A3.

Irradiated co-culture (Fibroblasts, ASCs, and MDA-MB-231) produces matrix with decreased collagen VI

The goal of this experiment was to test the proteomic make up of ECM generated by irradiated cells. The two groups tested herein are same as before (Figure 14); groups i and iii, cancer and healthy cocultures. Irradiation of the coculture groups i and iii, along with ASCs alone, fibroblasts alone, and MDA-MB-231 alone did not significantly effect viability of cells 24 hours later (**Figure 15**) allowing for further downstream testing with the same dosage and culture pattern.

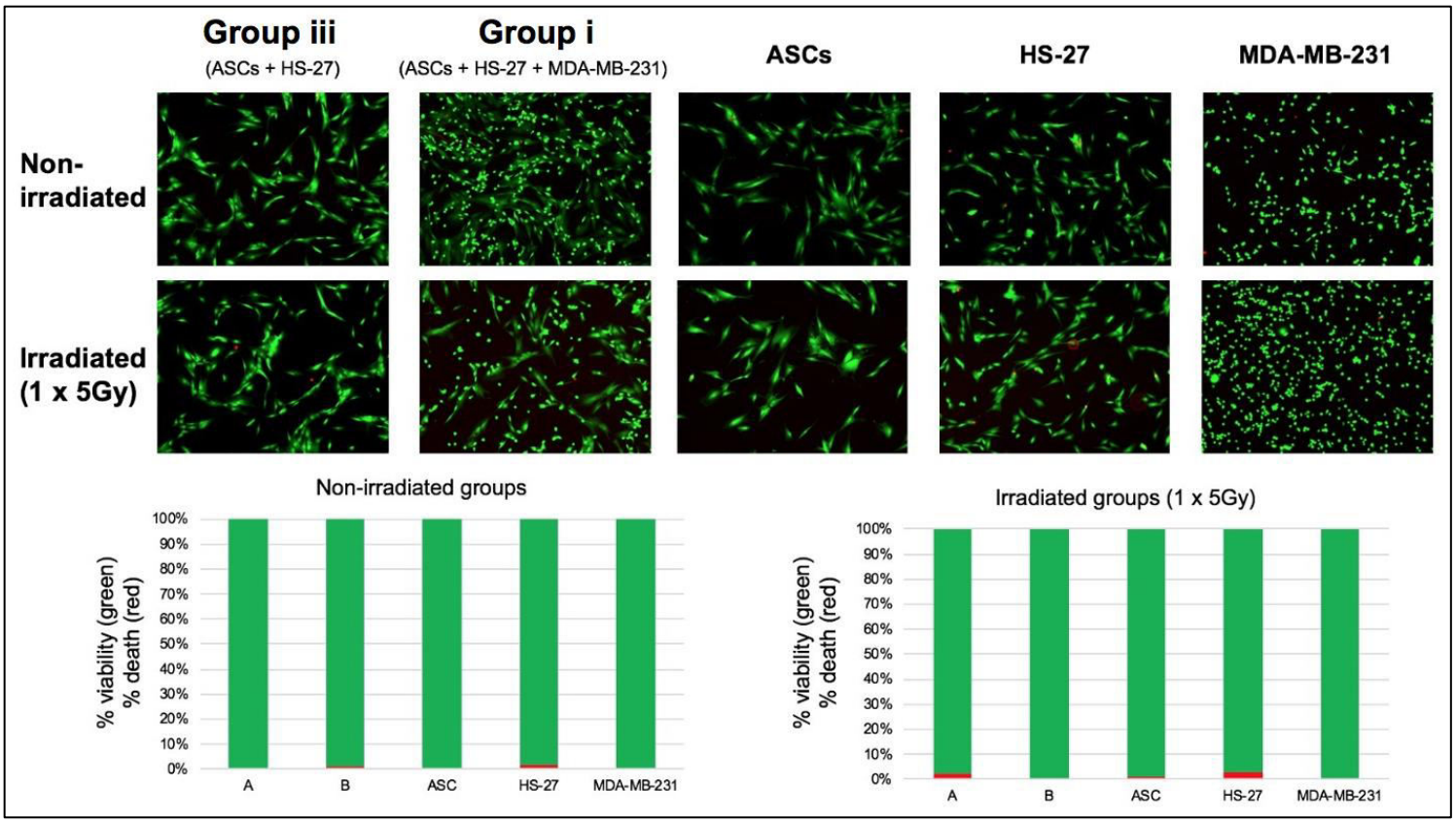

Figure 15: Analysis of radiation on cell viability. Top: Fluorescent micrographs of cells in non-irradiated and irradiated groups, separated per cell co-culture and cell monocultures. Below, proportional bar graphs showing quantified live/dead cells from irradiation. Group iii coculture and fibroblasts alone showed cell viability of approximately 97% in irradiated groups.

Irradiated cells of group i produce matrix that is low in collagen VI

Per **Figure 6**, the irradiation and matrix deposition protocol was followed. One week later, the matrix was decellularized, then recellularized with MDA-MB-231. After one day of culture, the cell/matrix combination was prepared for mass spectrometry. Proteomic analyses show that while the three strands of the collagen VI isoform were more abundant in the cancer matrix than the healthy matrix, these differences were not significant (**Figure 16**).

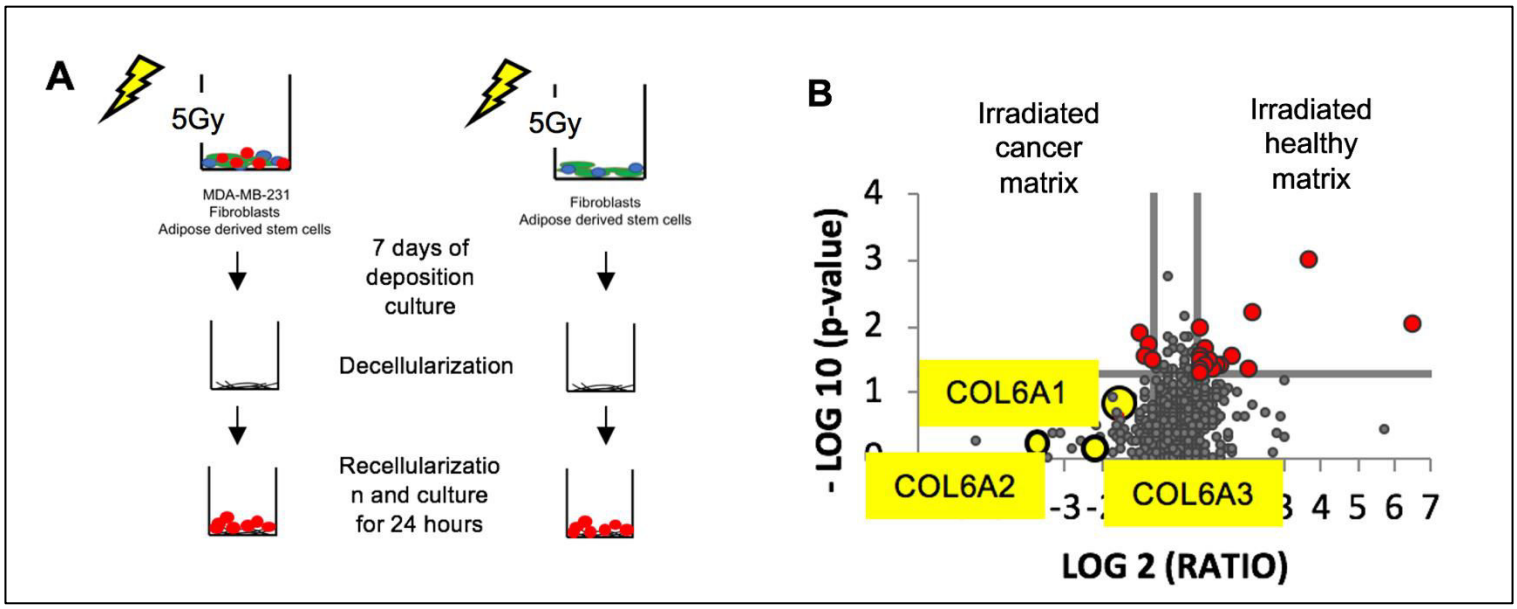

Figure 16: Schematic showing workflow for irradiated cell groups. A) Cells were seeded as normal, and irradiated 24 hours after seeding. Cells were cultured for one week, decellularized, and recellularized with MDA-MB-231. One day later, samples were prepared for mass spectroscopy. B) Volcano plot showing significantly differently abundant proteins in irradiated group i ('cancer matrix') versus irradiated group iii ('healthy matrix'). Three yellow data points below the horizontal line of significance represent the three strands of collagen VI, COL6A1, COL6A2 and COL6A3.

Human biopsy samples of triple negative tumors show long linear extensions of collagen from tumor, which stain positively for collagen VI

Human biopsy samples from TNBC tumors were sectioned and stained to investigate the tumor border *in vivo*. Samples were kindly provided by the Institute of Pathology on Trogerstrasse (Professor Karl Friedrich Becker).

TACS 3 structures found *in vivo*

H&E stains of human tumor samples taken from the tumor border (n = 3) clearly exhibited straight outgrowths of collagen (staining dark pink under H&E stain) from the tumor outwards into non-cancerous tissue (**Figure 17).**

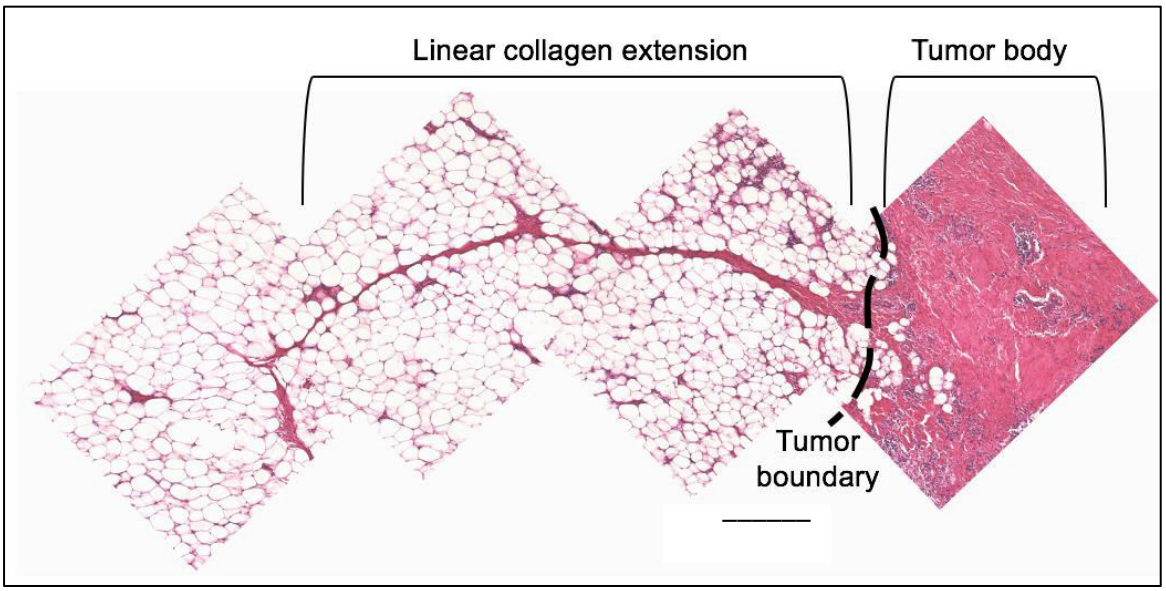

Figure 17: Histology taken from human *in vivo* TNBC tumor border. Compiled image of 4 micrographs stained with H&E to detect collagen. Linear outgrowth extends from tumor into parenchyma, is consistent with the description of tumor associated collagen signatures. Scale bar 100μm.

Linear collagen outgrowths stain positively for COL6

IHC of tumor samples (serially cut next to the H&E stained slides) stained positively for CCL5 and collagen VI (**Figure 18**). Importantly, there is positive DAPI staining along the outgrowth of collagen, implying the collagenous linear structures are cellular.

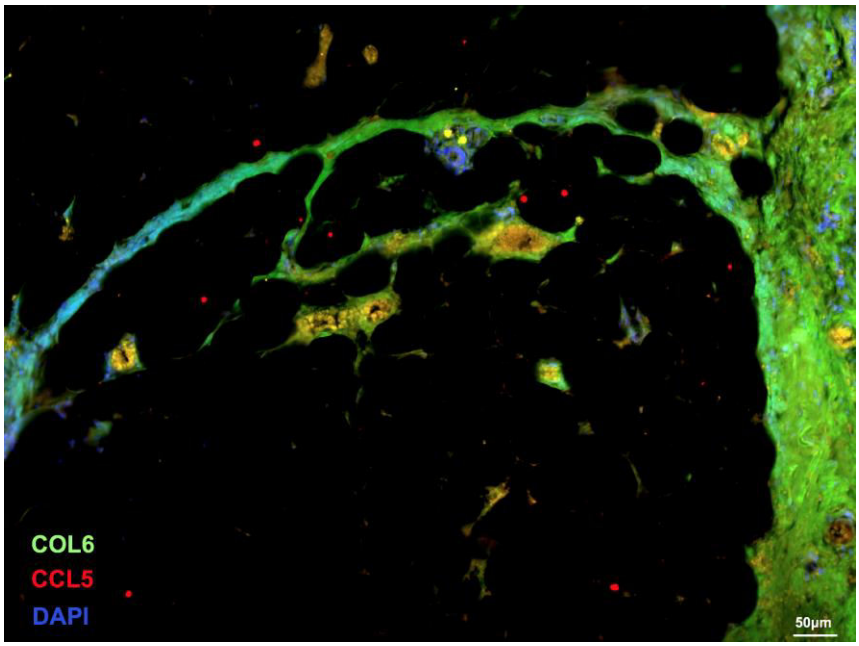

Figure 18: IHC of TNBC breast tumor border. Micrograph shows co-immunostaining for CCL5 (red), collagen type six (green), and DAPI (blue). Scale bar 50µm.

Cells reseeded on cancer matrix exhibit invasive behaviour

The aim of these experiments was to test the impact of the different ECMs on MDA-MB-231 cells, specifically looking at any enhancement of invasive behavior (road-like formation).

MDA-MB-231 cells reseeded self-organize into threads

By the fifth day of culture for the reseeded cells, the MDA-MB-231 cells growing on the decellularized matrix of group i formed road-like structures. On the decellularized matrices of groups i and iii, cells grew normally in a monolayer (**Fig 19A**). An example of such formations is shown in **Figure 19B**; some reseeded cells formed sophisticated continuous lines running 360-390µm.

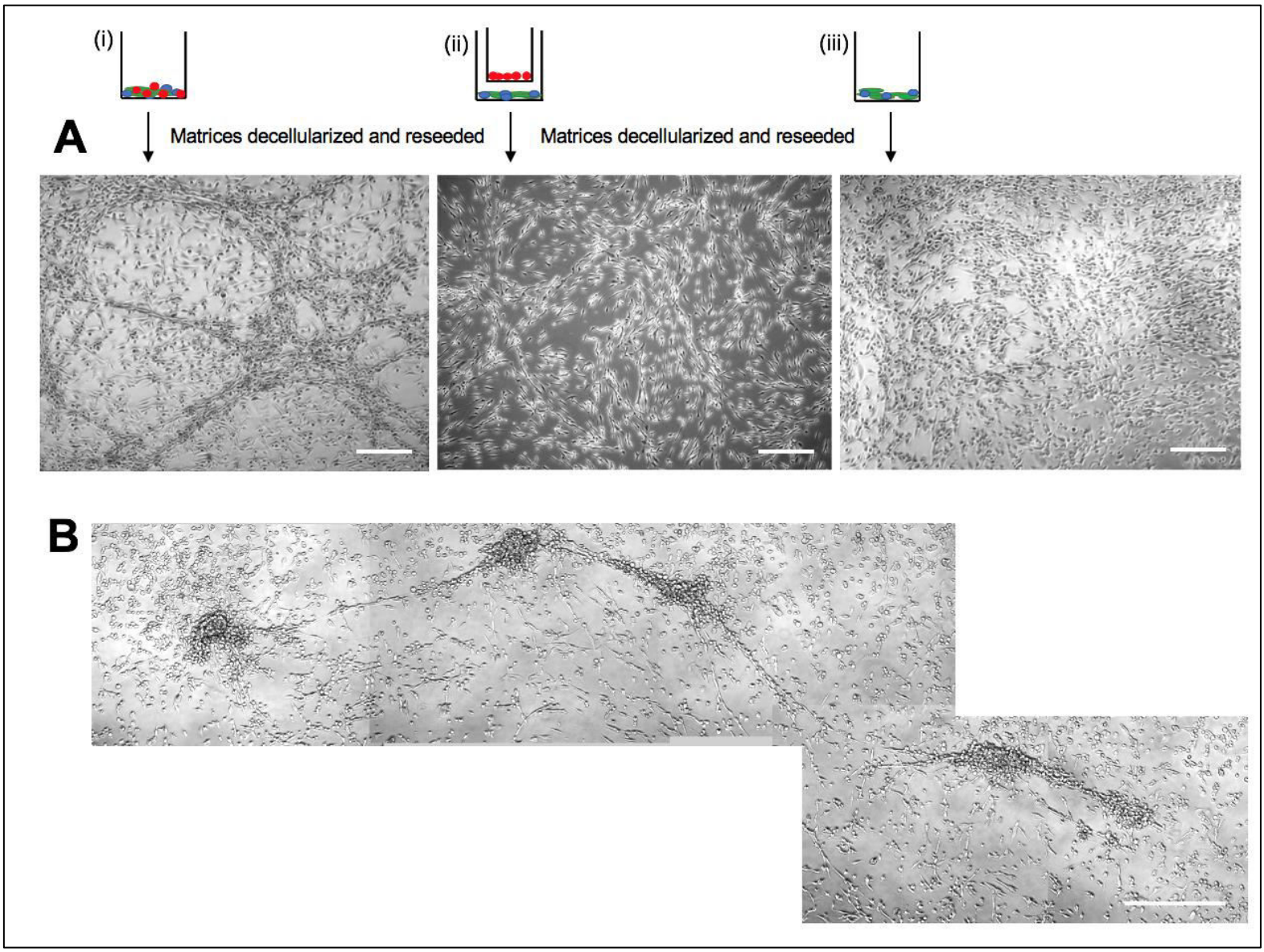

Figure 19: MDA-MB-231 morphologic response to reseeding on ECM. A) Brightfield images taken on day five of culturing reseeded cells on decellularized matrices. Scale bar 100µm. B) Example of contiguous linear cell structure orchestrated by the reseeded cells on decellularized matrix from group i. Scale bar 100µm.

MDA-MB-231 cells reseeded have insignificantly different pro-oncogenic transcriptional activity on matrix of group i compared to group iii

PCR analysis on MDA-MB-231 cells reseeded on ECM from group i showed higher gene expression of SLUG and IL-6, compared to MDA-MB-231 grown on matrices from

groups ii and iii. MMP3 did not vary significantly in reseeded cells across any of the decellularized matrices (**Figure 20**).

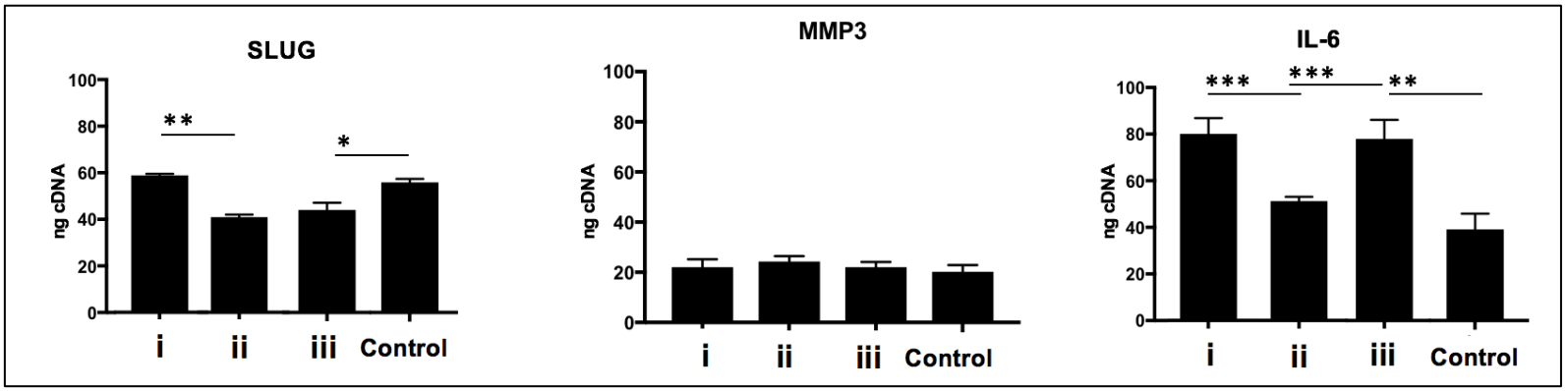

Figure 20: PCR results from MDA-MB-231 cells reseeded on matrices from groups i, ii, and iii, with a control group of MDA-MB-231 cells seeded on untreated dishes. Cells reseeded on matrix from group i has significantly higher levels of SLUG compared to groups ii and iii. Group i also has similar and high expression of IL-6 compared to group ii and control. MMP3 did not show any significant differences across all 4 groups. Error bars represent standard deviation (**$p < 0.01$, ***$p < 0.0001$).

Gene ontology term analysis of reseeded MDA-MB-231 cells reflects invasive behaviour

The top three gene ontology terms (GO terms) which matched the MDA-MB-231 cells reseeded on group i matrix featured 'cell cycle', 'cell movement', and 'post-translational modification' (**Figure 21**). Functional pathway analysis using string-db.org showed increased activity in both post-translational modification and transportation to rough endoplasmic reticulum (through RPS21, SRP9, GFM, and MRPS12) (which have been linked to breast cancer prognostics (109)).

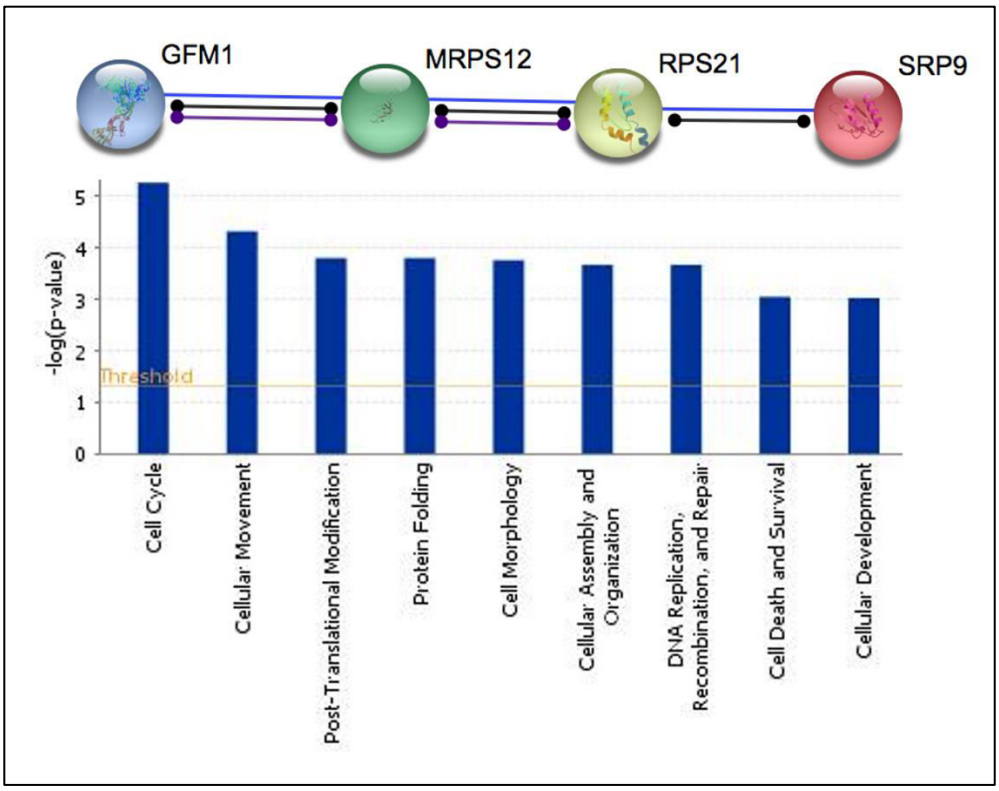

Figure 21: Gene ontology and functional pathway analysis. Top: String (string-db.org) data output highlighting most active intracellular pathways and proteins of reseeded cells on the matrix of group i. Bottom: Ingenuity Pathway Analysis data output showing top nine GO terms for reseeded cells on matrix of group i.

CCL5 is abundant in cultures where linear matrix is deposited

These experiments were run to investigate soluble markers present in the media while ECM is being deposited.

CCL5 highly upregulated in group i co-culture

A screen of 80 different cytokines in the media of the co-cultures during matrix deposition showed an increased level of CCL5 produced by group i (**Figure 22**). This datapoint presented a clear target for manipulation in further experiments.

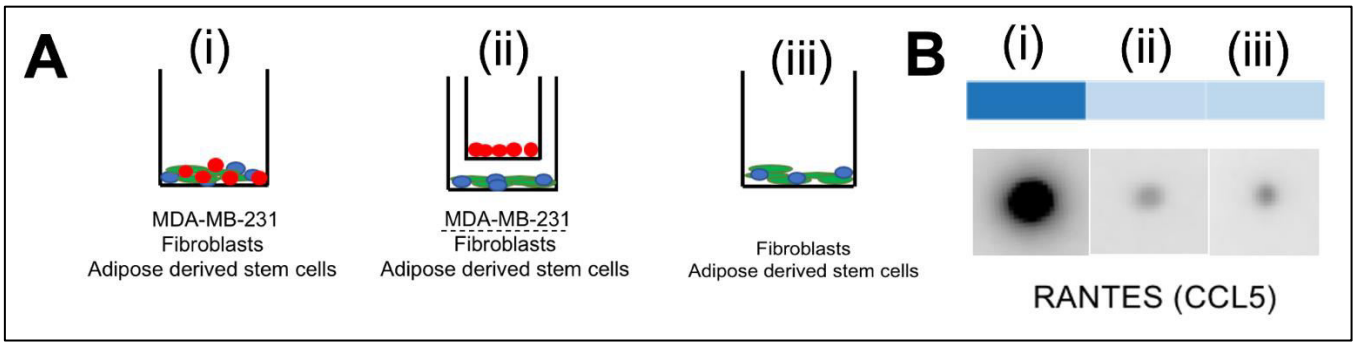

Figure 22: Cytokine analysis part I. A) Three schematics showing groups i, ii, and iii. B) the antibody detection blot for CCL5, quantified digitally in blue (top) and extracted from the micrograph (bottom).

IL-6 upregulated in co-cultures featuring MDA-MB-231

Using the same blot, IL-6 was also screened and seen to be more abundant in groups i and ii; the co-cultures featuring MDA-MB-231 (**Figure 23**).

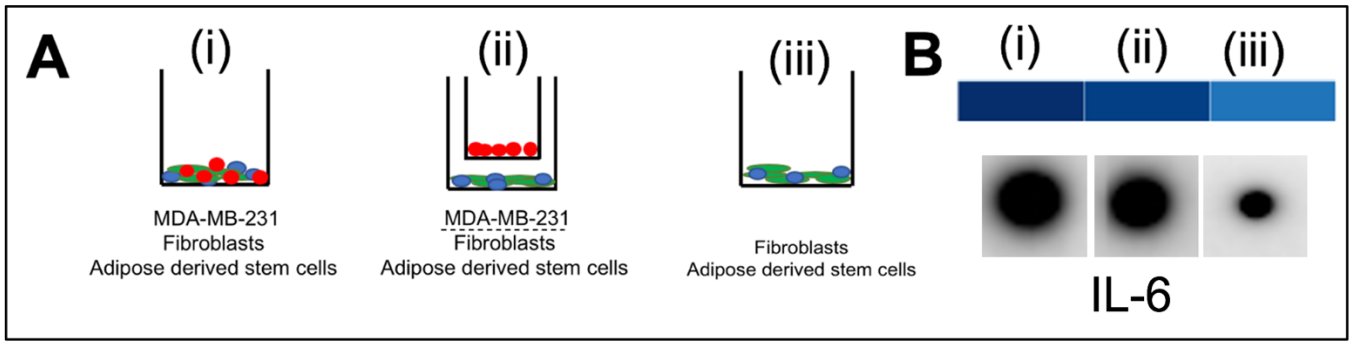

Figure 23: Cytokine analysis part II. Three schematics showing groups i, ii, and iii. B) the antibody detection blot for IL-6, quantified digitally in blue (top) and extracted from the micrograph (bottom).

Blocking CCL5 during matrix deposition prohibits linear matrix formation

Having established a large upregulation of CCL5 in the media of group i during matrix deposition, this experiment was to interfere with this signaling pathway to observe any causal effect of CCL5 on the linear morphology/collagen VI content of group i ECM.

Blocking CCL5 results in non-lethal physical isolation of cell types from one another

When monoclonal antibody against human CCL5 was supplied to the co-culture of group i during the seven day culture period, cells were observed as round, and not attached to the other cells in the vicinity. Despite obvious increased phase contrast of the cells through brightfield microscopy, a hallmark of cell culture apoptosis, a live/dead assay showed 100% cell viability (**Figure 24**).

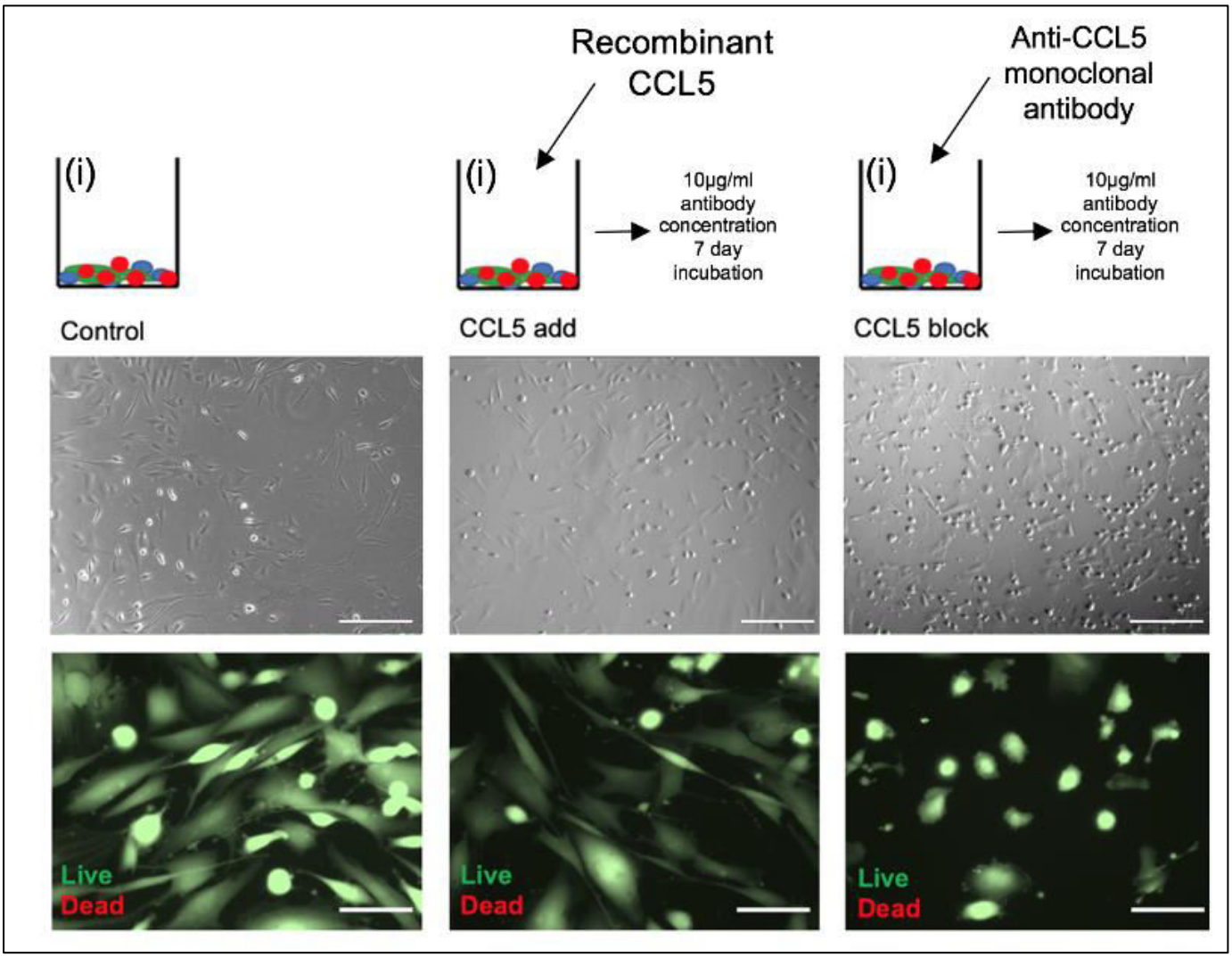

Figure 24: Cell viability assay after treatment with recombinant CCL5/CCL5 antibody. Top: Three schematics showing group i in its three conditions; control, CCL5 added, and CCL5 blocked. Underneath, brightfield images of co-culture reacting to each condition. Scale bar 100µm. Bottom: Viability stain on co-cultures at an increased magnification, showing full viability (all fluorescent green). Scale bar 50µm.

Decellularized matrix formed in CCL5-depleted environment is random and non-linear

Addition of recombinant CCL5 to group i and group iii cocultures did not induce deposition of a matrix that was significantly different to the control in terms of physical linearity and collagen VI staining. Conversely, blocking CCL5 in group i coculture induced significantly less matrix formation than the control (**p* = 0.041), and the proportion of collagen VI present was also dramatically decreased (**p* = 0.012) (**Figure 25**).

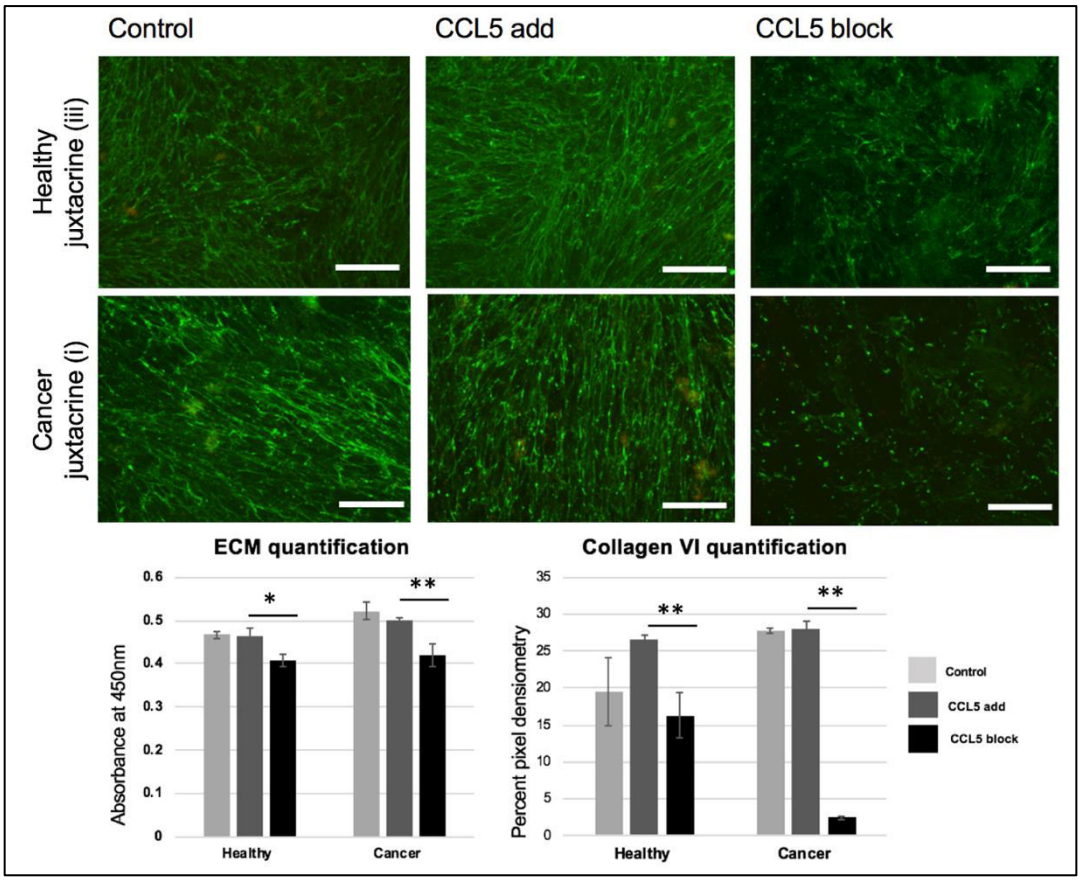

Figure 25: Analysis of collagen VI morphometry and quantity deposited *in vitro*. Images top to bottom: Fluorescent green micrographs are all staining for collagen VI. Top row = group iii during matrix deposition, bottom row = group i during matrix deposition. Images left to right: left = control group (no treatment), middle = recombinant CCL5 treatment, right = antibody against CCL5 treatment. Scale bar 100µm.
Below: Left graph: Quantification of matrices under treatment conditions. Right graph: Collagen VI quantification via pixel densiometry. (**p* <0.05, ***p* < 0.01).

Decellularized matrix formed in CCL5-depleted environment is low in collagen VI

The use of antibody against CCL5 as the matrices were being deposited resulted in an overall decrease in collagen VI of group i matrix ($^{**}p = 0.0049$). This was coupled with the decrease in overall ECM quantity ($^{**}p = 0.0044$) (**Figure 26**).

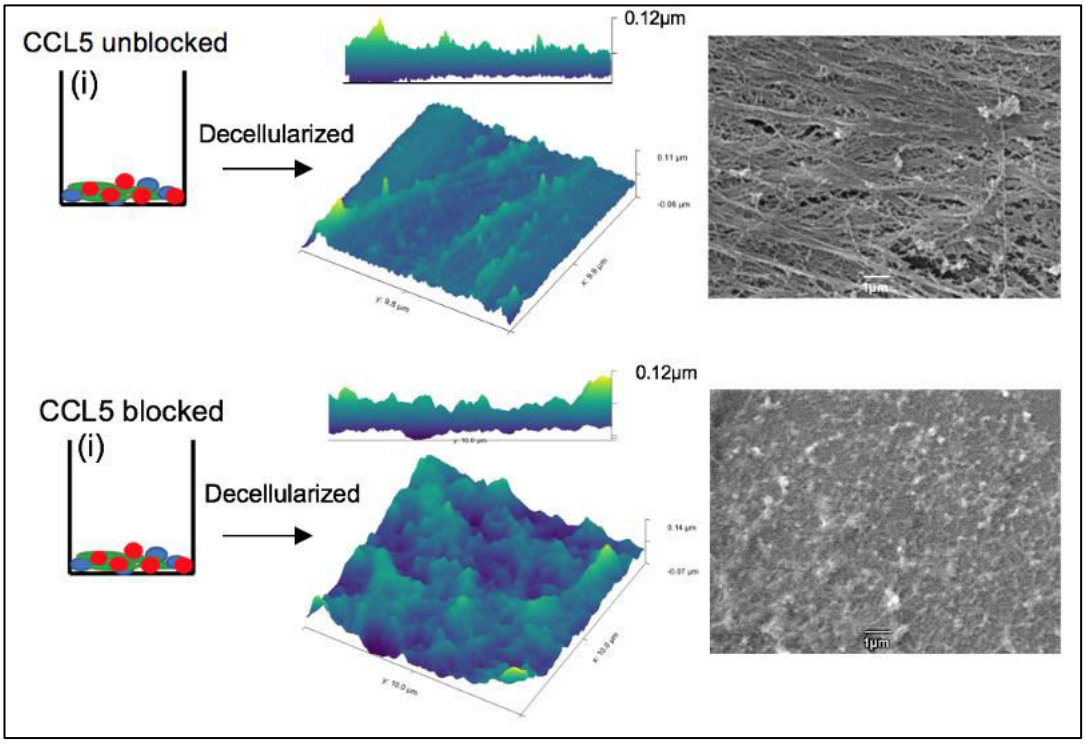

Figure 26: Blocking CCL5 leads to amorphous ECM deposition by group i culture. Left to right: Schematics of matrix deposition group i under two culture conditions; culture without CCL5 blocking antibody and culture with CCL5 blocking antibody. Middle panels show AFM micrographs of decellularized cultures, highlighting three dimensional differences of matrices achieved through blocking CCL5. Micrographs on the right from the SEM showing structural differences of matrices in detail.

Decellularized matrix formed in CCL5-depleted environment does not stimulate integrin β1 expression in reseeded MDA-MB-231 cells

The cells reseeded on decellularized matrix of group i generated with CCL5 blocker showed decreased expression of integrin β1, with cells growing in a normal monolayer. In comparison, reseeded cells on group i matrix generated with additional CCL5 self-assembled into linear structures, and had higher expression of integrin β1, which after

three days was significantly different (*p = 0.029, **Figure 27**). Integrin β1 strongly drives TNBC metastasis, and can act as a prognosticator of breast cancer (110). This was the rationale for targeted IHC stain.

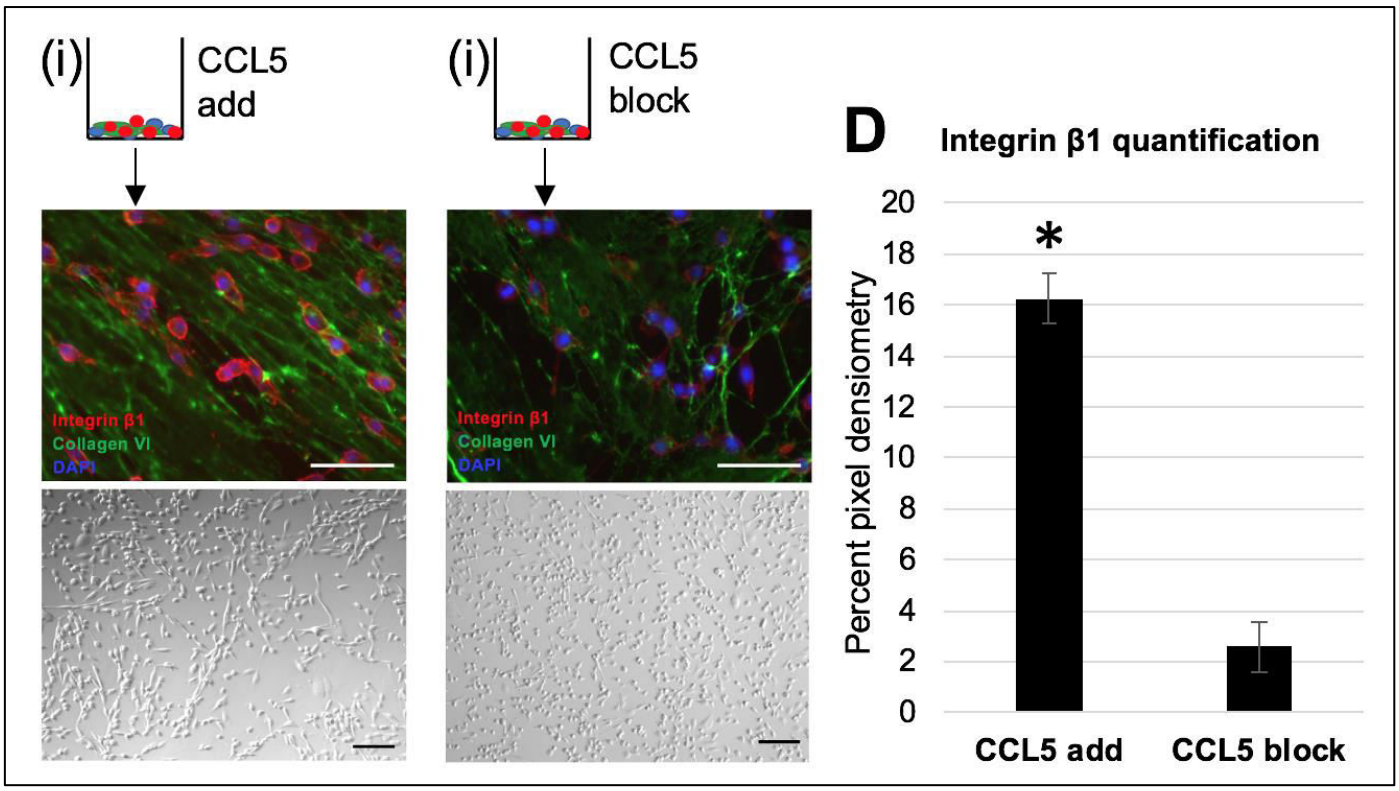

Figure 27: Integrin expression of reseeded MDA-MB-231 cells. Top left: schematics show group i co-cultures under different test conditions. Below: fluorescent images containing co-staining for integrin β1 (red), collagen VI (green), and DAPI (blue). Scale bar 50μm. Bottom micrographs: brightfield images of reseeded cells on treated matrices on day 3 of culture. Scale bar 100μm. Right: graph quantifying integrin β1 staining per pixel densiometry ($p < 0.05$).

Fibroblasts alone under paracrine influence of MDA-MB-231/ASC coculture produce linearized collagen VI

Since there was evidence that three cell types together generated CCL5 (MDA-MB-231/ ASCs/fibroblasts), while only two cell types (ASCs/fibroblasts) did not, it was important to parse the co-culture to see which exact cells are interacting together to create CCL5, and which are responsible for producing the linearized matrix.

Fibroblasts create linear collagen VI under influence of CCL5

The matrix which fibroblasts alone produce while receiving paracrine signals from a fibroblast/MDA-MB-231 mix is randomly arranged, and stains positively for collagen VI. However, the same fibroblast arrangement receiving paracrine signaling from a mix of ASC/MDA-MB-231 produce matrix which is highly linear and organized, also staining positively for collagen VI (**Figure 28a**).

CCL5 is generated mainly by ASC/MDA-MB-231 juxtacrine interaction

Gene expression analysis shows that a culture of ASC/MDA-MB-231 produces significantly higher CCL5 compared to fibroblast/MDA-MB-231 culture (*p <0.05) (**Figure 28b**). Conditioned media sampled while matrices were deposited (day five of culture period) has higher levels of detectable free CCL5 in the media of the ASC/MDA-MB-231 co-culture compared to conditioned media from a fibroblast/MDA-MB-231 co-culture (**Figure 28c**).

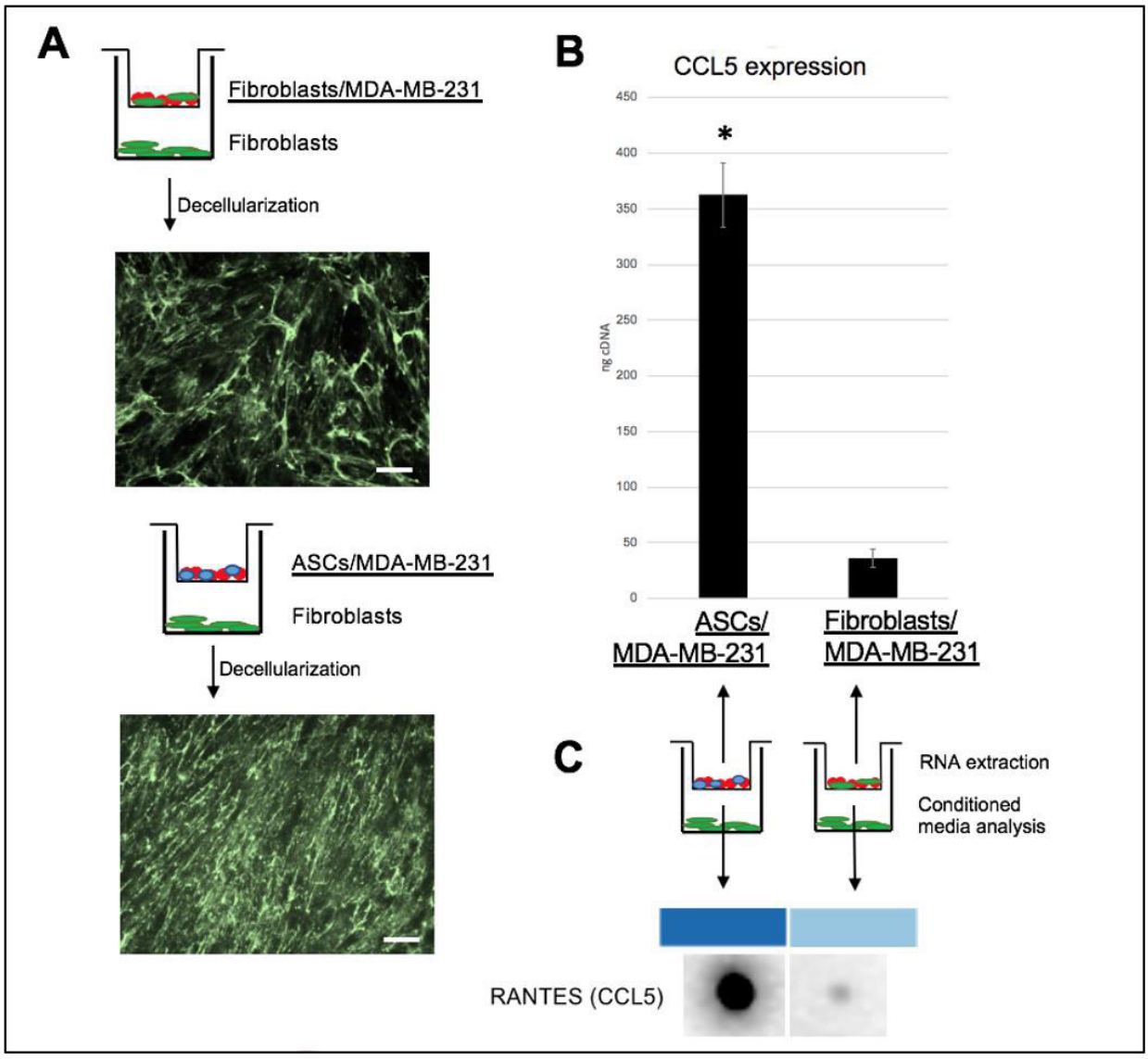

Figure 28: Analysis of source of CCL5, and main generator of linear collagen. A) Top: Schematic shows Boyden chamber culture of fibroblasts/MDA-MB-231 cells in the insert, having paracrine effect on underlying fibroblasts. Fluorescent image below is the IHC stain for collagen VI of decellularized matrix produced by fibroblasts. Matrix is unorganized. Scale bar 100μm. A) Bottom: Schematic shows Boyden chamber culture of ASCs/MDA-MB-231 cells in the insert, having paracrine effect on underlying fibroblasts. Fluorescent image below is the IHC stain for collagen VI of decellularized matrix produced by fibroblasts. Matrix is linear. Scale bar 100μm B) Bar graph depicts PCR results of amplifying CCL5 from ASC/MDA-MB-231 compared to fibroblast/MDA-MB-231. Standard deviation is shown by error bars. (*p <0.05). C) Chemiluminescent image extracted from array, corresponding to CCL5 detection blot. Comparison groups are conditioned media from ASC/MDA-MB-231 co-culture compared to fibroblast/MDA-MB-231 co-culture.

Evidence for unreported cell relationship in the creation of linear collagen of triple negative breast tumors

To conceptually draw the relationship which can be distilled from these data, it would involve showing the MDA-MB-231 cell population in juxtacrine contact with adipose derived stem cells (**Figure 29**). This relationship would produce CCL5, which is free to bind with CCR5 of fibroblast populations. The subsequent cascade of CCL5 fibroblast signaling produces a desmoplastic response, which leads to production of linearized collagen.

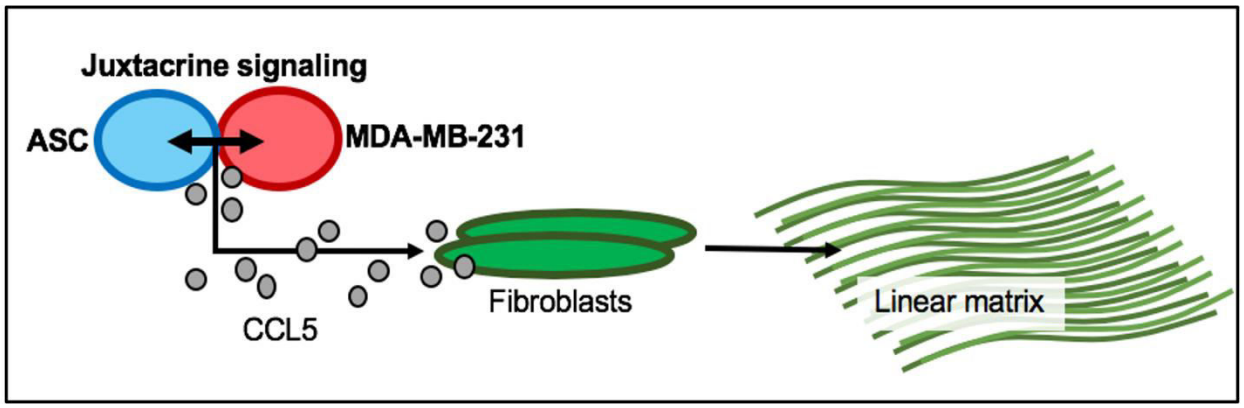

Figure 29: Introductory schematic to main, novel finding of this PhD project.
The proposed axis begins on the left with a known cellular relationship: ASC and MDA-MB-231 cells together produce CCL5. The CCL5 is free to act on local fibroblasts, which in turn produce a linearized matrix which is rich in collagen VI. This aspect has not been described before, and is the apex of this entire project.

Discussion

The data presented in this thesis, while solely *in vitro*, connect research on striated matrix (76), CCL5 (111), and collagen VI (112) of TNBC. To summarize the chief finding of this work, linear collagen type VI is produced by fibroblasts. It is dependent on CCL5, a cytokine produced by a juxtacrine culture of ASCs and MDA-MB-231 cells.

TACS3 in TNBC

Linear collagen radiating from the TNBC tumor is mirrored across multiple publications. Tumor associated collagen signatures was first described in 2006 by Patricia Keely of University of Wisonsin (76). It is a system which addresses three distinct layers of ECM which encapsulate the TNBC tumor. TACS1 is the innermost shell, characterized by densely packed collagen. TACS2 is a middle layer of collagen arranged in onion-like layers. TACS3 features the well described linear collagen which leads away from the tumor (76, 80), shown in **Figure 30.**

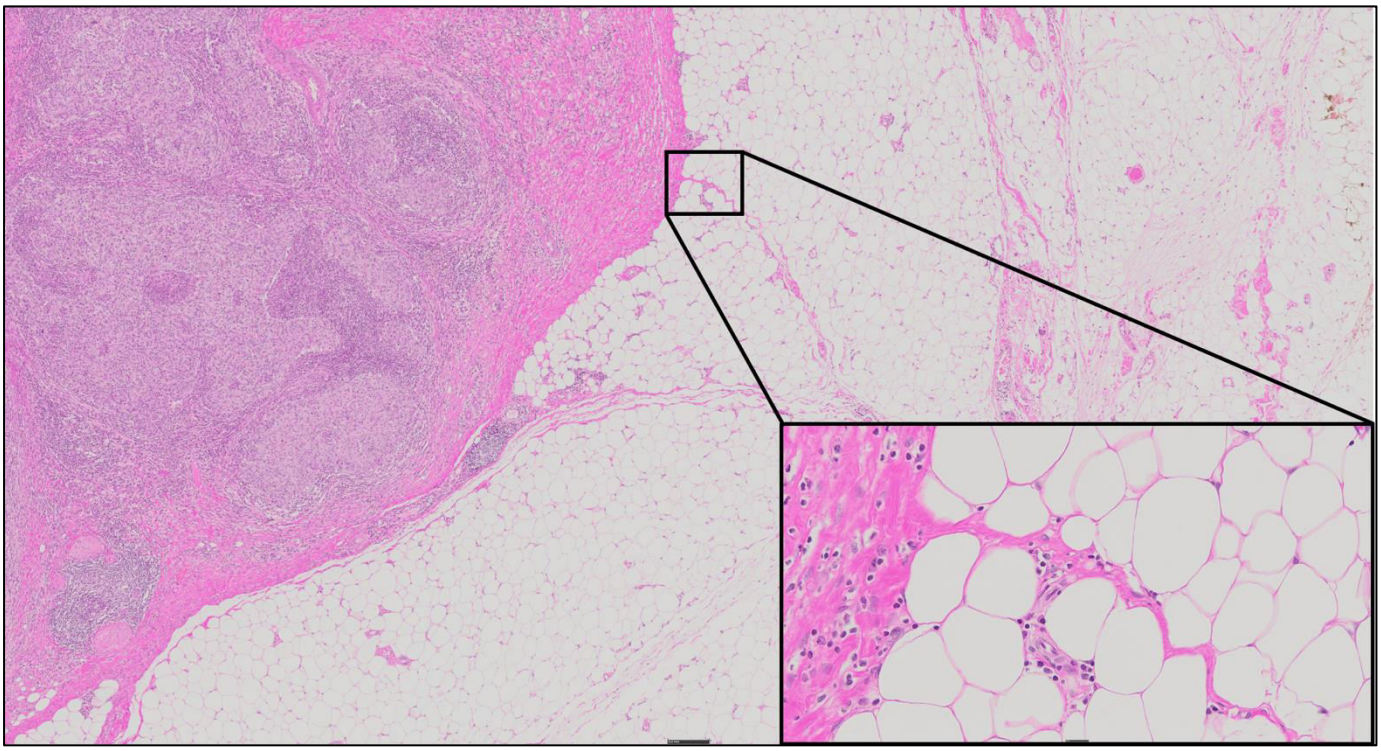

Figure 30: Example of TACS 3 *in vivo,* human tissue. Image shows border of invasive breast tumor, H&E stain. Zoomed in panel is an example of a linear outgrowth of collagen, coming from the tumor body. This is consistent with the pattern description of TACS3. Scale bar 500μm. University of Basel, *Pathorama.* (Used in accordance with guidelines; https://pathorama.ch/vslides/index.html).

While TACS is detectable using histological sections with classic picrosirius red staining and SHG (79), a study seeking to improve SHG for TACS visualization was performed in 2017. This work saw the value of TACS as a diagnostic model, but the general inaccessibility of second harmonic generation microscopy. The authors therefore aimed at performing label free, high-throughput, cheaper, more accessible spatial light interference microscopy (SLIM). It marks a step towards normalizing TACS diagnostics in histopathology labs (84).

It is reasonable to assume, based on the literature and data from this project, that the TNBC tumor contains high levels of collagen type VI. *In vivo* literature has shown that a col6a1$^{-/-}$ mouse crossed with MMTV-PyMT had decreased tumor hyperplasia and slowed formation of the primary tumor (113).

Linking the known facts: linear collagen at the tumor border, and collagen VI playing a role in tumor development, it becomes interesting to combine these two features and consider linear collagen type VI.

Collagen VI is generated by the triple negative breast tumor

Collagen VI is found ubiquitously around the body, and deposited in a meshwork fashion around skeletal muscle fascicles (114). Tendons represent a location in the body where collagen VI is found in a linear format. As such, the arrangement of collagen is not a mesh, but a striated tension-bearing type, designed with a mechanical off-loading purpose. Collagen VI is critical to healthy, functional tendon formation, exhibited clearly in col6$^{-/-}$ mice (115). The linear formation of the collagen VI is governed by a population of fibroblasts called tenocytes. Tenocytes are also responsible for creation of tenosynovial fluid, the lubricant which facilitates smooth passage of the tendon within its sheath (synovium), and formation of the synovium (inflamed in e.g. tenosynovitis) (116). The collagen forming tenocytes are known to be receptive to CCL5, in an inflammatory capacity (117). These studies together show that collagen VI microfibrils have a specifically linear phenotype, and are producible by fibroblasts under CCL5 signaling. The work of this thesis builds on an similar function of CCL5 signaling in breast cancer fibroblasts.

Collagen VI is known as a crucial component of breast cancer tumors. It has been seen that adipocyte-derived collagen VI concentration was high in developing triple negative breast tumors (118). In concert with increased hyaluronan synthesis from mammary epithelial cells, collagen VI is known to facilitate EMT. More than that, collagen VI has been localized to the invasive front of the tumor (112).

In terms of liquid biopsy research, MMP generated collagen VI fragments can be used as a reliable blood biomarkers in cancer patients compared to healthy controls (119). Collagen VI is a heterotrimer made of α1, α2, and α3 chains. The cleaved C5 domain of the α3 chain results in a peptide called endotrophin (ETP) (120). ETP is a pro-fibrotic chemoattractant, capable of guiding EMT and pro-angiogenic cell behavior. ETP can also induce chemoresistance to cisplatin, making it a therapeutic target (121). It appears the nature and location of collagen VI, and its degradation products, could confer an array of pro-oncogenic features to a growing tumor. In the data presented by this thesis, collagen VI was abundant in a non-biased screen of extracellular molecules from the cancer juxtacrine matrix by mass spectrometry. Using that result as a guide, targeted collagen VI antibody staining was extremely positive in the matrix made by group i; ASC/fibroblast/MDA-MB-231 cells cultured together. Also, the linear collagen at the tumor border of human biopsies stained positively for collagen VI. These results hint at the cell types responsible for the formation of collagen VI in TNBC.

Triple negative breast cancer cells use CCL5 for chemotaxis and linear collagen formation

CCL5 is a member of the C-C chemokine family, is also known as RANTES (‘regulated on activation, normal T cell expressed and secreted’). It acts as a potent chemoattractant of tumor associated macrophages (TAMs), eosinophils, basophils, and T cells (122). CCL5 is a ligand for G-protein coupled receptors CCR1, CCR3 and CCR5. However, in breast cancer signaling, the main receptor/ligand pairing is CCL5/CCR5 (123).

CCL5 is an important factor in the binding of endothelial cell membranes (124) specifically, acting together with the transmembrane proteins CD44 and syndecan-1 (CD138) (125, 126), to bind T-cell membranes to lymphoid endothelia. It was observed

in the CCL5 blocking experiments that the blocking antibody in the co-culture resulted in fibroblasts, ASCs and MDA-MB-231 cells physically isolating themselves from one another. It can be hypothesized that the normal cell-binding role of CCL5 is also hindered here. Extrapolating, the last set of results show high CCL5 production only by membrane-membrane contact of ASCs and MDA-MB-231 cells together. It is possible, based on this evidence, that there is a positive feedback loop in place; where CCL5 is required to attach the membranes of ASCs and MDA-MB-231, allowing the cell types to produce free CCL5 from the juxtacrine relationship.

In normal physiology, CCL5 is in high concentration in breast milk, specifically in early colostrum (127), and is responsible for attracting maternal circulating leukocytes into breast milk for neonatal transfer (128). This indicates overall that the breast is able to create large amounts of CCL5 under the correct stimuli. In the tumor, CCL5 is highly produced and can act in a range of pro-oncogenic ways (129, 130). It has been validated that tumor associated CCL5 is significantly sourced from local mesenchymal stem cells (111). The literature is unified regarding the pro-invasive, pro-metastatic impact of CCL5 on breast tumors (122, 131). For instance, CCL5 *in situ* within the tumor biopsy has been correlated with stage II breast cancer (132). Meanwhile, the amount of freely circulating CCL5 was reported to increase with each invaded lymph node in breast cancer patients (133-135). In this project, an antibody against CCL5 is used to successfully disrupt the formation of linear collagen type VI. Extrapolating to *in vivo* studies, this might be an explanation for why administration of monoclonal antibody against CCL5 (intraperitoneally in mouse) showed a reduction in breast tumor metastasis (111). There are multiple research pathways exploring the reduction of CCL5 as a breast cancer therapy. The HIV drug Maraviroc acts as a competitive antagonist for CCR5, aimed at limiting T-cell CD44 signaling via CCL5 (136). Research *in silico* (137) and *in vivo* (mouse) (138) have shown the theoretical and practical usage of Maraviroc on reducing both primary tumor growth rates and metastasis. Even a patent for the pivoted use of Maraviroc to TNBC treatment was filed in 2012 (patent #CA2873743A1). However, as with the majority of studies manipulating CCL5, the structure of the tumor is not examined or considered. The effect of CCL5 on the creation of linear matrix has never been described, nor unfortunately has there been much attention paid to the

possible impact of CCL5 on tumor construction. This thesis aims to connect these fields of work together for the first time.

TNBC uses structural linearity to promote invasion

In the years that followed the work describing TACS, there have been satellite studies eluding to the collagen signatures put forth in 2006. In 2016, a novel gradient based *in vitro* model was described, involving a 2mg/ml collagen type 1 gel loaded with MDA-MB-231 cancer cells, interfaced with a more rigid 10mg/ml Matrigel, separated by a basement membrane analogue. It was seen that MDA-MB-231 cells not only manipulated the collagen type 1 into a linearized format, but these collagen fibers directed the breast cancer cells out into the acellular, denser Matrigel (78). Importantly, this same study ran the model with non-invasive MCF-7 breast cancer cells, and observed weak cellular migration and invasion. In corroboration with this, a 2018 study observed microstructural statistics on the fibers penetrating dense Matrigel. They noted that oriented fibers *in vitro* can efficiently transmit long-range cellular tracks, enhancing migration of cancer cells (139). In 2019, a study was run on the supportive role of non-malignant cells themselves in guiding cancer cell protrusions into controlled 3D environments *in vitro.* The novel models involved tumor spheroids containing cancer-associated fibroblasts (CAFs) and cancer cells in a 1.9mg/ml collagen type 1 solution. Cancer cells (pancreatic, lung adenocarcinoma) bound to cancer associated fibroblasts (CAFs) via integrin $\alpha 5\beta 1$, providing force which converted to cancer cell invasion into acellular collagen gel (140). This study showed cancer cells traveling with linear extensions of fibroblasts, which adds to the framework of the tumor using physical linearity to invade. In the data of this thesis, there were road-like structures formed by the reseeded MDA-MB-231 cells. It is likely the cells are preferentially growing along the linear structures, however, it does show how matrix can be a blueprint for cell invasion, even *in vitro.*

Linear collagen VI benefits tumor progression

Since this is a relatively new field of research, started in 2006 (76), there can be many different interpretations as to why the invasive breast tumor would benefit from linear

collagen outgrowths. Returning to keystone cancer publications can help to guide scientific analysis. Hanahan and Weinberg (141) identify 'activating invasion and metastasis' as one hallmark of cancer. TACS3 is an extremely clear tableau of this particular characteristic. Similarly, ETP, a breakdown product of collagen VI, serves as a pro-angiogenic, which fulfils the hallmark of 'inducing angiogenesis'. 'Avoiding immune destruction' is achieved by cancer cells reaching the healthy extracellular milieu. TACS3 structures also serve to expand the three dimensional tumor range, especially in breast tumors which are known for rapid growth (142). Another characteristic of tumor development per Hanahan & Weinberg is evasion of growth suppressors. Contact inhibition is a phenomenon which arrests cell division when cell density reached a critical threshold (143). The formation of physical structures which allow the tumor to ferry out cells gives a neat option for a tumor to avoid critical hyperplasia, which would normally have to battle contact inhibition.

It has been known for a decade that linear collagen at the tumor border helps the tumor to reach nearby blood vessels and all the resources therein (144), thereby avoiding hypoxia related stresses, accessing oxygen and a gateway to metastasize (145).

On a clinical level, it is advantageous for the tumor to very discreetly extend itself through the healthy parenchyma and stroma, especially since TACS3 is difficult to detect. TACS3 affords the tumor a better chance of surviving the treatment combination administered, and recurring, which generally happens between 1-3 years later (146, 147). For these reasons, it is beneficial for the tumor to build such opportunistic, linear structures.

Irradiation reduces cancer cell growth and induces formation of a less oncogenic ECM

Irradiation frequently accompanies chemotherapy in the treatment of TNBC, and when performed, is associated with better survival rates of patients (148). Doses of radiation range from 1000-5000cGy (149), which is fractionated over the course of five to six weeks (150). The cells in the irradiation data of this research received a one-time dose of 5Gy, consistent with the literature (151), and which did not significantly affect the viability of the cells, seen in the presented data within this thesis. Considering the anti-

cancer effect of irradiation, it is interesting to observe that the irradiated cells themselves tend to produce a matrix which is lower in collagen VI than its non-irradiated comparison. This hints at the influence of radiation on the cells in making a microenvironment which is less oncogenic than its non-irradiated comparison. A valuable next experiment would be to test CCL5 production by an irradiated co-culture of ASCs/MDA-MB-231, to investigate if this stage in the linear matrix deposition is impacted by irradiation. After all, a reduction of CCL5 means a decrease in a sequelae of pro-oncogenic events which is known to be a result of radiation in TNBC (152). Importantly, ASCs have been seen to be relatively robust in their response to irradiation; both in the present data and literature (153). This helps explain the high therapeutic efficacy of fresh ASCs in grafted fat under irradiated skin, which serve as tool to rescue the fibrotic phenotype of chronic dermal radiation damage (154).

ECM turnover is balanced by proteolysis and suppression of collagen production

The tumor is a heterotypic structure with high microenvironment plasticity. While CCL5 is known to act in a paracrine manner for monocyte and macrophage attraction to the tumor (155), the work of this thesis eludes to a specific, non-fibrotic paracrine effect of MDA-MB-231 on the resident non-cancer cell populations. Considering the traffic of cells into and out of the tumor mass (129), it would make sense the microenvironment of the tumor is not purely pro-fibrotic. MMP1 (156) and MMP9 (157) are proteases upregulated in triple negative breast tumors, and work in concert with pro-fibrotic cytokines to balance turnover as the tumor expands (158). However, the data listed in figures 12 and 13 of this thesis show little/no matrix deposited by the fibroblasts/ASCs under paracrine influence of MDA-MB-231 alone. This could reflect a relationship whereby collagen production is not stimulated as strongly when TNBC cells act in a paracrine manner with the classic collagen producing cells. Considered from an *in vivo* perspective, this would translate into strategic cessation of ECM production, creating a looser microenvironment and facilitating ease of passage for infiltrating cells and chemokines; a hallmark of invasive tumors (159). Similarly, the penetration of TACS3 structures coming from the tumor boundary itself would be unencumbered by a less

dense zone surrounding the tumor. There is evidence that fibrosis is pro-oncogenic (160), but not necessarily that cancer itself is extremely pro-fibrotic (161). Data within the current thesis highlights that not all paracrine mechanisms of breast cancer are pro-fibrotic, allowing the assumption that there is a balancing system against heavy pro-fibrotic mechanisms.

The ASC and MDA-MB-231 juxtacrine connection is highly oncogenic

There are many descriptions of the paracrine role of mesenchymal stem cells in cancer development, and a wealth of scientific evidence testing it. However, it is difficult to say anything definitive about the cellular relationship, partly due to the complex nature of stem cell research and patient-to-patient variability (162). The ASC is of mesenchymal origin, but resides within adipose tissue to give rise to a range of soft tissue/connective tissue structures (163, 164). Like MSCs, ASCs can differentiate along lineages of adipocytes, chondrocytes, muscle cells, and vascular endothelial cells (165). There is a complex reciprocal dialogue between MSCs and MDA-MB-231, for instance, MSCs are powerful metastatic drivers of MDA-MB-231, via MCP-1 (166). It has been seen that MDA-MB-231 can cause CCL5 secretion from MSCs through NF-κB signaling (167). NF-κB pathway is a known driver of CCL5 expression through p50 (168), alongside Jun N-terminal Kinase (JNK) signaling (169) and mitogen activated protein kinases (MAPK) pathway (170). These signaling pathways are known to be upregulated in MSC/MDA-MB-231 interactions (171, 172). In terms of functionality, an admixture of MDA-MB-231 and MSCs orthotopically injected resulted in increased production of CCL5 and highly metastatic tumors *in vivo,* while MDA-MB-231 and fibroblasts together did not lead to increased primary tumor development or lung metastases. This indicates a unique partner role of the stem cell to the cancer cell (111). This same study determined that only a juxtacrine, not paracrine, relationship of MDA/MB-231 and MSCs resulted in an upregulation of CCL5, mirroring the same finding here in the cytokine array studies. Overall, there is a large body of evidence that resident stem cells and TNBC cells act together through various pathways to produce CCL5.

IL-6 has been reported as another cytokine secreted in concert with CCL5 by MSCs, to potentiate a pro-invasive TNBC phenotype (173). And, congruent with present findings,

was highly upregulated in the media of group i (cancer juxtacrine group). Importantly, IL-6 is seen produced by fibroblasts downstream of CCL5 (specifically, synovial fibroblasts) (174). The findings of this thesis indicate that knock-on fibroblastic IL-6 production was activated by triple negative breast cancer cells, and thus it becomes important to consider the effect of CCL5 on construction of fibroblast-generated ECM.

CCL5-stimulated fibroblasts are sufficient generators of collagen VI

IL-6 is a known driver of fibrosis in inflammation (175), scar tissue deposition (176), liver cirrhosis (177), and gastric cancer fibrosis (178). As an intervention, it has been seen that strategic blocking of IL-6 *in vivo* ameliorates lung fibrosis (179). IL-6 shares the same desmoplastic function in breast tumors (180, 181), which can act as a positive feedback loop for breast cancer, as BC development has been seen to be triggered by obesity associated breast fibrosis (182).

CCL5 acting in concert with IL-6 is known to occur in the breast cancer setting, and has been examined before. Specifically, Maraviroc (anti-CCL5) and tocilizumab (anti-IL-6) used as a combination therapy were together more effective than either drug alone in reducing tumor size and metastasis *in vivo* (183). Since IL-6 is known to induce collagen deposition, and since the data presented in this thesis elude to a mechanism where the collagen is linear only with CCL5, it raises the question of whether CCL5 plays a role in spatially guiding the collagen deposition stimulated by IL-6.

Rationale for future development of this research field

As it stands, TACS3 as a tool appears to strongly fit the purpose of invasion and metastasis (78, 80, 141). It so follows that identifying the exact makeup of the TACS3 collagen could be of direct clinical and surgical benefit. However, the existing scientific literature does not have sufficient depth. For instance, the literature involves *in vitro* collagen gels made of collagen type 1. The *in vitro* assays therefore bias the study of TACS towards collagen type 1, rather than *de novo* creation of collagen as a tumor model (140). Meanwhile, *in vivo* collagen labelling is not specific to collagen type, but limited to picrosirius red staining and SHG (77). The exact proteomic makeup of the TACS are unknown. The research platforms needed to investigate TACS further will

require a larger animal model to allow accurate ECM formation (e.g. pig), and *in vitro* work which allows *de novo* creation of ECM, rather the prescribed collagen isoforms and structures. To be more direct, this work is pointing directly at the blocking of CCL5 as a mainstay of TNBC treatment. Given the lack of side effects from blocking the CCL5 pathway, and since the existing drug is highly tolerable to the patient, a clinical trial of the CCR5-blocking HIV drug Maraviroc in TNBC has precedent (184). From a surgical standpoint, the molecular identification of TACS3 could change what is considered an R0 (margin negative) resection. Considering that an R0 resection can still recur up to 12% after 10 years, there is room for improvement, and a precedent for further TACS investigation (57). If histopathology shows TACS3, it is probable there are already metastases, and cancer cells disseminated further in the breast (81, 96). There is compelling reason to direct attention towards adjuvant/neoadjuvant therapeutics to limit TACS3 development.

Consequences for surgical practices derived from this research

The field of breast cancer surgery is wide and changing annually. Two major points to link this thesis with are 1) fat grafting, and 2) R0 resections.

1) The fear of introducing adipose tissue to a post-mastectomy/lumpectomy zone, via fat grafting, has been well documented (163). The *in vitro* work of most publications has used a Boyden chamber to illustrate the pro-oncogenic cytokines upregulated in the paracrine relationship between ASCs and MDA-MB-231. The preliminary experiments of this thesis tested the Boyden chamber assay with another migration assay of my own design, which was published in 2019 (185). The goal of this work was to assess the relationship of the ASC and MDA-MB-231 cell in a new way. The novel migration assay did not recapitulate the pro-oncogenic paracrine profile of the classical Boyden chamber assays. However, further experiments of the ECM arm of this thesis, showed that once connected, a pro-oncogenic effect of juxtacrine ASC/MDA-MB-231 is seen in the form of CCL5 upregulation. It seems that while the ASCs are migrating towards the cancer cell population, there is not a detectable oncogenic paracrine profile, compared to the extremely upregulated CCL5 production when the ASCs finally arrive at the cancer cell

membranes. These *in vitro* assays have shed light on the dual-nature of the paracrine/juxtacrine relationship of ASC/MDA-MB-231, and helps to explain the disparity in the literature.

Fat grafting has a valuable place in breast reconstructive surgery. Specifically, post-radiation, skin can become extremely fibrotic and accompany loss of underlying volume. Fat grafting underneath can restore skin quality and elasticity, along with replenishing lost volume (154, 186, 187).

2) In terms of surgical excision of breast tumors, the goal of the oncologists is an R0 resection; meaning the margins around the removed tumor are microscopically examined, and there are no detectable cancer cells present. Classically, 'no ink on tumor' is the criteria used by pathologists to confirm full removal of cancer cells. Briefly, the surgeon excises tissue suspected to contain the tumor in its entirety, and stains the sides of the tissue with different colors of ink, so as to orient the pathologist. The tissue is handed over to the pathologist who processes it for histology immediately, while the patient is still on the table. The rule of thumb is that if no cancer cells are seen to touch the ink, and are 1mm away from the inky border, an R0 resection has been achieved (58, 188). This work is performed within a 30 minute window, and based on the ink color, the surgeon is spatially guided in real time which aspect of the tumor may need to have a deeper cut. This universally used standard is based purely on cellular detection rather than ECM anomalies.

As the current 'ink on tumor' criteria focuses purely on the cellular tumor border, it is important to address how this technique might evolve with ECM tumor border. The work of this thesis readdresses the concept of 'ink on tumor'; asking if a further histological investigation step for collagen type VI should be also performed. Remnants of TACS3 are cellular themselves, and it is worth asking if TACS3 are potentially camouflaging cancer cells from histopathologists.

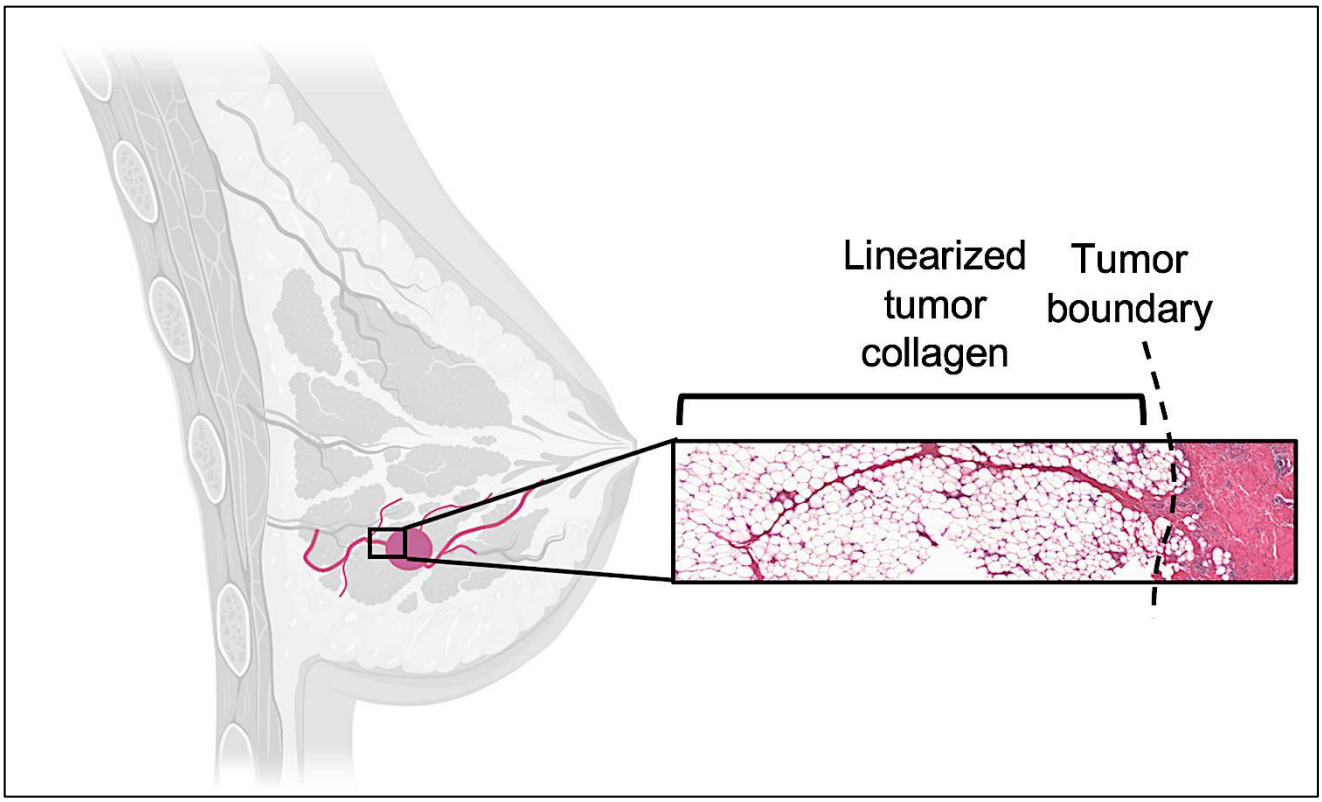

Figure 31: Situation of TNBC tumor *in vivo,* highlighting breast tissue planes. (Left) schematic showing breast tumor *in situ,* represented by pink color. Lines from pink tumor body indicate collagenous outgrowths/tumor moving along planes of soft tissue in the breast. Made with biorender.com. (Right) micrograph isolated from histology section taken at the tumor boundary, H&E staining, representing how the tumor appears at the edge. Dotted line represents the tumor boundary, tumor lies to the right of the line, TACS3 linear collagen on the left.

Limitations and future aims

The work of this project is mainly *in vitro*, with one *in vivo* arm which correlates human histology with the findings of lab experiments. This work is limited by the lack of an animal model. While there is an intervention arm (CCL5 blocking), it too is *in vitro*, and there is no pharmacological aspect to this work (e.g. drug use (Maraviroc)).

The literature indicates using Maraviroc as an agent to limit tumor formation. This could feasibly be considered at any point in the breast cancer therapeutic plan, as it is a relatively innocuous drug and could theoretically be used in every case worldwide to inhibit tumor formation/metastasis/recurrence. The use of animal models should be limited to large animals (e.g. pigs/sheep) given the detail needed on the tumor boundary

– a difficult parameter to study in the miniscule mouse mammary gland. However, an animal model would enable intervention studies as well as full structural analysis of the tumor and mammary gland; not possible in human studies.

A range of clinical science can arise from this work. Surgical resections could include collagen VI staining. Study on the anti-fibrotic paracrine effect of MDA-MB-231 could enlighten tumor heterogeneity and drug targeting. A study with CCL5 and radiotherapy could help decrease the fibrotic nature of irradiated breasts; a known barrier to accurate diagnostics (189).

Conclusion

The most coherent hypothesis to be supported by the present dataset is that there is a paracrine relationship between ASCs and MDA-MB-231 cells, which produces CCL5 in high amounts. The CCL5 acts on fibroblasts, to stimulate the production of linear ECM, high in collagen VI. It is already known that CCL5 plays a pro-oncogenic role, via chemoattraction of cells to the tumor. The chief supposition of this *in vitro* work is that there is another, unreported role to CCL5 in TNBC; the construction of linear collagen VI at the boundary of the tumor. This collagen format is known to the world as TACS3, and before now, there was no explanation for its formation. The work of this thesis has provided a link for the first time to CCL5, collagen VI at the tumor boundary, and TACS3 linear collagen formation.

Acknowledgements

This work would not exist without my team of collaborators, supervisors, and my loved ones backstage. I had the honor and pleasure of working with multiple different facilities in Munich and my home town of Galway, Ireland.

Dr. Micheal Rosemann, Dr. Omid Azimzadeh, and Professor Michael Atkinson of the Helmholtz Institute ran mass spectrometry analyses on my samples, and pushed me to run the best possible project I could.

Dr. Juliane Merl-Pham gave me her time for a 1:1 tutorial on mass spectrometry and proteomic analysis. She and Dr. Stefanie Hauck of PROT analyzed my proteomic data and shared their limitless expertise.

Professor Kerin and Professor Lowery took me under their wing in the Lambe Institute in my hometown of Galway. Their agreement to host me and my project for the month of April 2019 was a special privilege. Dr. Éadaoin Timmins provided AFM data. She has analyzed samples I shipped from Munich to Ireland; I am grateful she shared her flexibility and plasticity of skill with me.

I humbly received antibodies from Professor Peter Nelson of LMU, and histology samples from Professor Karl Friedrich Becker. I thank them for their generosity and interest in my work. Ilse Schunn of Medical Materials and Implants provided me with wonderful SEM images – I thank her profusely.

Professor Machens took me in from the very start; I am forever grateful for the opportunity and unwavering support. Professor Krüger went from my Molecular Oncology lecturer to a trusted advisor and colleague. I thank him for taking a chance on me in the early days, and for sharing expertise along the way. Dr. Huemer allowed me to observe breast surgery in his clinic, and was a key person in the design of this project. Together, these three experts formed my advisory board. Their contributions guided me through, and it was a true pleasure to work with each of them.

From meeting Dominik Duscher in Stanford in 2014, he has picked me up on my bad days, celebrated the good, and motivated me in between. I am forever grateful he chose me to add into his group as a PhD student.

Matthias Sauter began his doctoral thesis with Dr. Duscher the same time as I did. We would work together consistently for 2.5 years, publish papers, and travel to Linz, Vienna, London, Helsinki, and Baltimore for conferences. He has been my right hand for the entirety of the PhD program. I consider him a lifelong friend and thank him for his genius and laughs.
Rachel Nuttall & Claire Doyle are my two confidants and mental health harbors. Daniel Hügenell is my ever-patient, understanding partner. Mary, Ger, and Siobhán Brett; my mother, father and sister, are the cornerstone of my life. Thank you all forever.

References

1. Khan YS SH. Anatomy, Thorax, Mammary Gland. StatPearls Publishing. 2019.
2. Javed A, Lteif A. Development of the human breast. Semin Plast Surg. 2013;27(1):5-12.
3. Peltenburg AL, Erich WB, Bernink MJ, Zonderland ML, Huisveld IA. Biological maturation, body composition, and growth of female gymnasts and control groups of schoolgirls and girl swimmers, aged 8 to 14 years: a cross-sectional survey of 1064 girls. Int J Sports Med. 1984;5(1):36-42.
4. Georgopoulos N, Markou K, Theodoropoulou A, Paraskevopoulou P, Varaki L, Kazantzi Z, et al. Growth and pubertal development in elite female rhythmic gymnasts. J Clin Endocrinol Metab. 1999;84(12):4525-30.
5. Apou G, Schaadt NS, Naegel B, Forestier G, Schonmeyer R, Feuerhake F, et al. Detection of lobular structures in normal breast tissue. Comput Biol Med. 2016;74:91-102.
6. Hefel L, Schwabegger A, Ninkovic M, Wechselberger G, Moriggl B, Waldenberger P, et al. Internal mammary vessels: anatomical and clinical considerations. Br J Plast Surg. 1995;48(8):527-32.
7. Shahoud JS KC, Burns B. Anatomy, Thorax, Internal Mammary (Internal Thoracic) Arteries. StatPearls Publishing. 2020 Apr 13.
8. Gherghe M, Bordea C, Blidaru A. Sentinel lymph node biopsy (SLNB) vs. axillary lymph node dissection (ALND) in the current surgical treatment of early stage breast cancer. J Med Life. 2015;8(2):176-80.
9. Hochhegger B, Langer FW, Irion K, Souza A, Moreira J, Baldisserotto M, et al. Pulmonary Acinus: Understanding the Computed Tomography Findings from an Acinar Perspective. Lung. 2019;197(3):259-65.
10. Tzu J, Marinkovich MP. Bridging structure with function: structural, regulatory, and developmental role of laminins. Int J Biochem Cell Biol. 2008;40(2):199-214.
11. Vidi PA, Bissell MJ, Lelièvre SA. Three-dimensional culture of human breast epithelial cells: the how and the why. Methods Mol Biol. 2013;945:193-219.
12. Gudjonsson T, Adriance MC, Sternlicht MD, Petersen OW, Bissell MJ. Myoepithelial cells: their origin and function in breast morphogenesis and neoplasia. J Mammary Gland Biol Neoplasia. 2005;10(3):261-72.
13. Cardoso F, Harbeck N, Fallowfield L, Kyriakides S, Senkus E. Locally recurrent or metastatic breast cancer: ESMO Clinical Practice Guidelines for diagnosis, treatment and follow-up. Ann Oncol. 2012;23 Suppl 7:vii11-9.
14. Elsedfy H. A clinical approach to benign breast lesions in female adolescents. Acta Biomed. 2017;88(2):214-21.
15. Neville G, Neill CO, Murphy R, Corrigan M, Redmond PH, Feeley L, et al. Is excision biopsy of fibroadenomas based solely on size criteria warranted? Breast J. 2018;24(6):981-5.
16. Ajmal M VFK. Breast Fibroadenoma. StatPearls Publishing. 2019 Nov.
17. Dion L, Racin A, Brousse S, Beltjens F, Cauchois A, Leveque J, et al. Atypical epithelial hyperplasia of the breast: state of the art. Expert Rev Anticancer Ther. 2016;16(9):943-53.
18. Felipe Lima J, Nofech-Mozes S, Bayani J, Bartlett JM. EMT in Breast Carcinoma-A Review. J Clin Med. 2016;5(7).
19. Egorov V, Kearney T, Pollak SB, Rohatgi C, Sarvazyan N, Airapetian S, et al. Differentiation of benign and malignant breast lesions by mechanical imaging. Breast Cancer Res Treat. 2009;118(1):67-80.
20. Barroso-Sousa R, Metzger-Filho O. Differences between invasive lobular and invasive ductal carcinoma of the breast: results and therapeutic implications. Ther Adv Med Oncol. 2016;8(4):261-6.
21. Tiang S, Metcalf C, Dissanayake D, Wylie E. Malignant hyperechoic breast lesions at ultrasound: A pictorial essay. J Med Imaging Radiat Oncol. 2016;60(4):506-13.

22. Gómez Macías GS, Pérez Saucedo JE, Cardona Huerta S, Garza Montemayor M, Villarreal Garza C, García Hernández I. Invasive lobular carcinoma of the breast with extracellular mucin: A case report. Int J Surg Case Rep. 2016;25:33-6.
23. McCart Reed AE, Kutasovic JR, Lakhani SR, Simpson PT. Invasive lobular carcinoma of the breast: morphology, biomarkers and 'omics. Breast Cancer Res. 2015;17(1):12.
24. Mehanna J, Haddad FG, Eid R, Lambertini M, Kourie HR. Triple-negative breast cancer: current perspective on the evolving therapeutic landscape. Int J Womens Health. 2019;11:431-7.
25. Lehmann BD, Bauer JA, Chen X, Sanders ME, Chakravarthy AB, Shyr Y, et al. Identification of human triple-negative breast cancer subtypes and preclinical models for selection of targeted therapies. J Clin Invest. 2011;121(7):2750-67.
26. Nielsen TO, Hsu FD, Jensen K, Cheang M, Karaca G, Hu Z, et al. Immunohistochemical and clinical characterization of the basal-like subtype of invasive breast carcinoma. Clin Cancer Res. 2004;10(16):5367-74.
27. Ellard SL, Clemons M, Gelmon KA, Norris B, Kennecke H, Chia S, et al. Randomized phase II study comparing two schedules of everolimus in patients with recurrent/metastatic breast cancer: NCIC Clinical Trials Group IND.163. J Clin Oncol. 2009;27(27):4536-41.
28. Finn RS, Dering J, Ginther C, Wilson CA, Glaspy P, Tchekmedyian N, et al. Dasatinib, an orally active small molecule inhibitor of both the src and abl kinases, selectively inhibits growth of basal-type/"triple-negative" breast cancer cell lines growing in vitro. Breast Cancer Res Treat. 2007;105(3):319-26.
29. Al-Thoubaity FK. Molecular classification of breast cancer: A retrospective cohort study. Ann Med Surg (Lond). 2020;49:44-8.
30. Makki J. Diversity of Breast Carcinoma: Histological Subtypes and Clinical Relevance. Clin Med Insights Pathol. 2015;8:23-31.
31. Reddy SM, Barcenas CH, Sinha AK, Hsu L, Moulder SL, Tripathy D, et al. Long-term survival outcomes of triple-receptor negative breast cancer survivors who are disease free at 5 years and relationship with low hormone receptor positivity. Br J Cancer. 2018;118(1):17-23.
32. Scott LC, Mobley LR, Kuo TM, Il'yasova D. Update on triple-negative breast cancer disparities for the United States: A population-based study from the United States Cancer Statistics database, 2010 through 2014. Cancer. 2019;125(19):3412-7.
33. Plasilova ML, Hayse B, Killelea BK, Horowitz NR, Chagpar AB, Lannin DR. Features of triple-negative breast cancer: Analysis of 38,813 cases from the national cancer database. Medicine (Baltimore). 2016;95(35):e4614.
34. Haffty BG, Yang Q, Reiss M, Kearney T, Higgins SA, Weidhaas J, et al. Locoregional relapse and distant metastasis in conservatively managed triple negative early-stage breast cancer. J Clin Oncol. 2006;24(36):5652-7.
35. Phipps AI, Buist DS, Malone KE, Barlow WE, Porter PL, Kerlikowske K, et al. Family history of breast cancer in first-degree relatives and triple-negative breast cancer risk. Breast Cancer Res Treat. 2011;126(3):671-8.
36. ElShamy WM. The protective effect of longer duration of breastfeeding against pregnancy-associated triple negative breast cancer. Oncotarget. 2016;7(33):53941-50.
37. Daling JR, Malone KE, Doody DR, Anderson BO, Porter PL. The relation of reproductive factors to mortality from breast cancer. Cancer Epidemiol Biomarkers Prev. 2002;11(3):235-41.
38. Keleher AJ, Theriault RL, Gwyn KM, Hunt KK, Stelling CB, Singletary SE, et al. Multidisciplinary management of breast cancer concurrent with pregnancy. J Am Coll Surg. 2002;194(1):54-64.
39. Greenup R, Buchanan A, Lorizio W, Rhoads K, Chan S, Leedom T, et al. Prevalence of BRCA mutations among women with triple-negative breast cancer (TNBC) in a genetic counseling cohort. Ann Surg Oncol. 2013;20(10):3254-8.

40. Daum H, Peretz T, Laufer N. BRCA mutations and reproduction. Fertil Steril. 2018;109(1):33-8.
41. Venkitaraman AR. Functions of BRCA1 and BRCA2 in the biological response to DNA damage. J Cell Sci. 2001;114(Pt 20):3591-8.
42. Britt K, Ashworth A, Smalley M. Pregnancy and the risk of breast cancer. Endocr Relat Cancer. 2007;14(4):907-33.
43. Husby A, Wohlfahrt J, Øyen N, Melbye M. Pregnancy duration and breast cancer risk. Nat Commun. 2018;9(1):4255.
44. Katz TA. Potential Mechanisms underlying the Protective Effect of Pregnancy against Breast Cancer: A Focus on the IGF Pathway. Front Oncol. 2016;6:228.
45. Lee CI, Chen LE, Elmore JG. Risk-based Breast Cancer Screening: Implications of Breast Density. Med Clin North Am. 2017;101(4):725-41.
46. Barkan D, El Touny LH, Michalowski AM, Smith JA, Chu I, Davis AS, et al. Metastatic growth from dormant cells induced by a col-I-enriched fibrotic environment. Cancer Res. 2010;70(14):5706-16.
47. Picon-Ruiz M, Morata-Tarifa C, Valle-Goffin JJ, Friedman ER, Slingerland JM. Obesity and adverse breast cancer risk and outcome: Mechanistic insights and strategies for intervention. CA Cancer J Clin. 2017;67(5):378-97.
48. McManus MJ, Welsch CW. The effect of estrogen, progesterone, thyroxine, and human placental lactogen on DNA synthesis of human breast ductal epithelium maintained in athymic nude mice. Cancer. 1984;54(9):1920-7.
49. Travis RC, Key TJ. Oestrogen exposure and breast cancer risk. Breast Cancer Res. 2003;5(5):239-47.
50. Gao H, Yang BJ, Li N, Feng LM, Shi XY, Zhao WH, et al. Bisphenol A and hormone-associated cancers: current progress and perspectives. Medicine (Baltimore). 2015;94(1):e211.
51. Sprague BL, Trentham-Dietz A, Hedman CJ, Wang J, Hemming JD, Hampton JM, et al. Circulating serum xenoestrogens and mammographic breast density. Breast Cancer Res. 2013;15(3):R45.
52. Di Cello F, Flowers VL, Li H, Vecchio-Pagan B, Gordon B, Harbom K, et al. Cigarette smoke induces epithelial to mesenchymal transition and increases the metastatic ability of breast cancer cells. Mol Cancer. 2013;12:90.
53. Kispert S, McHowat J. Recent insights into cigarette smoking as a lifestyle risk factor for breast cancer. Breast Cancer (Dove Med Press). 2017;9:127-32.
54. Wang RX, Chen S, Jin X, Shao ZM. Value of Ki-67 expression in triple-negative breast cancer before and after neoadjuvant chemotherapy with weekly paclitaxel plus carboplatin. Sci Rep. 2016;6:30091.
55. Wu Q, Ma G, Deng Y, Luo W, Zhao Y, Li W, et al. Prognostic Value of Ki-67 in Patients With Resected Triple-Negative Breast Cancer: A Meta-Analysis. Front Oncol. 2019;9:1068.
56. Wahba HA, El-Hadaad HA. Current approaches in treatment of triple-negative breast cancer. Cancer Biol Med. 2015;12(2):106-16.
57. Dunst J, Dellas K. Margins! Margins. Margins? How Important Is Margin Status in Breast-Preserving Therapy? Breast Care (Basel). 2011;6(5):359-62.
58. Lombardi A, Pastore E, Maggi S, Stanzani G, Vitale V, Romano C, et al. Positive margins (R1) risk factors in breast cancer conservative surgery. Breast Cancer (Dove Med Press). 2019;11:243-8.
59. Kamel D, Gray C, Walia JS, Kumar V. PARP Inhibitor Drugs in the Treatment of Breast, Ovarian, Prostate and Pancreatic Cancers: An Update of Clinical Trials. Curr Drug Targets. 2018;19(1):21-37.
60. Collignon J, Lousberg L, Schroeder H, Jerusalem G. Triple-negative breast cancer: treatment challenges and solutions. Breast Cancer (Dove Med Press). 2016;8:93-107.
61. Miller K, Wang M, Gralow J, Dickler M, Cobleigh M, Perez EA, et al. Paclitaxel plus bevacizumab versus paclitaxel alone for metastatic breast cancer. N Engl J Med. 2007;357(26):2666-76.
62. Weaver BA. How Taxol/paclitaxel kills cancer cells. Mol Biol Cell. 2014;25(18):2677-81.

63. Pollhammer MS, Duscher D, Schmidt M, Huemer GM. Recent advances in microvascular autologous breast reconstruction after ablative tumor surgery. World J Clin Oncol. 2016;7(1):114-21.
64. Goodenough CJ RJ. Breast Transverse rectus abdominus muscle (TRAM). StatPearls Publishing. 2016 June.
65. Sood R, Easow JM, Konopka G, Panthaki ZJ. Latissimus Dorsi Flap in Breast Reconstruction: Recent Innovations in the Workhorse Flap. Cancer Control. 2018;25(1):1073274817744638.
66. Bellini E, Pesce M, Santi P, Raposio E. Two-Stage Tissue-Expander Breast Reconstruction: A Focus on the Surgical Technique. Biomed Res Int. 2017;2017:1791546.
67. Uda H, Tomioka YK, Sugawara Y, Sarukawa S, Sunaga A. Shaping of the Unaffected Breast with Brava-Assisted Autologous Fat Grafting to Obtain Symmetry after Breast Reconstruction. Aesthet Surg J. 2015;35(5):565-73.
68. Mestak O, Mestak J, Bohac M, Edriss A, Sukop A. Breast Reconstruction after a Bilateral Mastectomy Using the BRAVA Expansion System and Fat Grafting. Plast Reconstr Surg Glob Open. 2013;1(8):e71.
69. Chung MT, Paik KJ, Atashroo DA, Hyun JS, McArdle A, Senarath-Yapa K, et al. Studies in fat grafting: Part I. Effects of injection technique on in vitro fat viability and in vivo volume retention. Plast Reconstr Surg. 2014;134(1):29-38.
70. Atashroo D, Raphel J, Chung MT, Paik KJ, Parisi-Amon A, McArdle A, et al. Studies in fat grafting: Part II. Effects of injection mechanics on material properties of fat. Plast Reconstr Surg. 2014;134(1):39-46.
71. Brett EA, Aitzetmüller MM, Sauter MA, Huemer GM, Machens HG, Duscher D. Breast cancer recurrence after reconstruction: know thine enemy. Oncotarget. 2018;9(45):27895-906.
72. Freese KE, Kokai L, Edwards RP, Philips BJ, Sheikh MA, Kelley J, et al. Adipose-derived stems cells and their role in human cancer development, growth, progression, and metastasis: a systematic review. Cancer Res. 2015;75(7):1161-8.
73. Bielli A, Scioli MG, Gentile P, Agostinelli S, Tarquini C, Cervelli V, et al. Adult adipose-derived stem cells and breast cancer: a controversial relationship. Springerplus. 2014;3:345.
74. Eterno V, Zambelli A, Pavesi L, Villani L, Zanini V, Petrolo G, et al. Adipose-derived Mesenchymal Stem Cells (ASCs) may favour breast cancer recurrence via HGF/c-Met signaling. Oncotarget. 2014;5(3):613-33.
75. Koellensperger E, Bonnert LC, Zoernig I, Marme F, Sandmann S, Germann G, et al. The impact of human adipose tissue-derived stem cells on breast cancer cells: implications for cell-assisted lipotransfers in breast reconstruction. Stem Cell Res Ther. 2017;8(1):121.
76. Provenzano PP, Eliceiri KW, Campbell JM, Inman DR, White JG, Keely PJ. Collagen reorganization at the tumor-stromal interface facilitates local invasion. BMC Med. 2006;4(1):38.
77. Case A, Brisson BK, Durham AC, Rosen S, Monslow J, Buza E, et al. Identification of prognostic collagen signatures and potential therapeutic stromal targets in canine mammary gland carcinoma. PLoS One. 2017;12(7):e0180448.
78. Han W, Chen S, Yuan W, Fan Q, Tian J, Wang X, et al. Oriented collagen fibers direct tumor cell intravasation. Proceedings of the National Academy of Sciences. 2016;113(40):11208-13.
79. Bancelin S, Nazac A, Ibrahim BH, Dokladal P, Decenciere E, Teig B, et al. Determination of collagen fiber orientation in histological slides using Mueller microscopy and validation by second harmonic generation imaging. Opt Express. 2014;22(19):22561-74.
80. Conklin MW, Eickhoff JC, Riching KM, Pehlke CA, Eliceiri KW, Provenzano PP, et al. Aligned collagen is a prognostic signature for survival in human breast carcinoma. Am J Pathol. 2011;178(3):1221-32.
81. Bredfeldt JS, Liu Y, Conklin MW, Keely PJ, Mackie TR, Eliceiri KW. Automated quantification of aligned collagen for human breast carcinoma prognosis. J Pathol Inform. 2014;5(1):28.

82. Golaraei A, Kontenis L, Cisek R, Tokarz D, Done SJ, Wilson BC, et al. Changes of collagen ultrastructure in breast cancer tissue determined by second-harmonic generation double Stokes-Mueller polarimetric microscopy. Biomed Opt Express. 2016;7(10):4054-68.
83. Han W, Chen S, Yuan W, Fan Q, Tian J, Wang X, et al. Oriented collagen fibers direct tumor cell intravasation. Proc Natl Acad Sci U S A. 2016;113(40):11208-13.
84. Majeed H, Okoro C, Kajdacsy-Balla A, Toussaint KC, Jr., Popescu G. Quantifying collagen fiber orientation in breast cancer using quantitative phase imaging. J Biomed Opt. 2017;22(4):46004.
85. Pavithra V SS, Rao RS, Patil S, Augustine D, Haragannavar VC, Nambiar S. Tumor-associated Collagen Signatures: An Insight. World Journal of Dentistry. 2017;8(3):224-30.
86. Kenny TC, Schmidt H, Adelson K, Hoshida Y, Koh AP, Shah N, et al. Patient-derived Interstitial Fluids and Predisposition to Aggressive Sporadic Breast Cancer through Collagen Remodeling and Inactivation of p53. Clin Cancer Res. 2017;23(18):5446-59.
87. Okoro C, Kelkar V, Sivaguru M, Emmadi R, Toussaint KC, Jr. Second-harmonic patterned polarization-analyzed reflection confocal microscopy of stromal collagen in benign and malignant breast tissues. Sci Rep. 2018;8(1):16243.
88. Tomko LA, Hill RC, Barrett A, Szulczewski JM, Conklin MW, Eliceiri KW, et al. Targeted matrisome analysis identifies thrombospondin-2 and tenascin-C in aligned collagen stroma from invasive breast carcinoma. Sci Rep. 2018;8(1):12941.
89. Emon B, Bauer J, Jain Y, Jung B, Saif T. Biophysics of Tumor Microenvironment and Cancer Metastasis - A Mini Review. Comput Struct Biotechnol J. 2018;16:279-87.
90. Esbona K, Yi Y, Saha S, Yu M, Van Doorn RR, Conklin MW, et al. The Presence of Cyclooxygenase 2, Tumor-Associated Macrophages, and Collagen Alignment as Prognostic Markers for Invasive Breast Carcinoma Patients. Am J Pathol. 2018;188(3):559-73.
91. Conklin MW, Gangnon RE, Sprague BL, Van Gemert L, Hampton JM, Eliceiri KW, et al. Collagen Alignment as a Predictor of Recurrence after Ductal Carcinoma In Situ. Cancer Epidemiol Biomarkers Prev. 2018;27(2):138-45.
92. Azimzade Y, Saberi AA, Sahimi M. Regulation of migration of chemotactic tumor cells by the spatial distribution of collagen fiber orientation. Phys Rev E. 2019;99(6-1):062414.
93. Xu S, Xu H, Wang W, Li S, Li H, Li T, et al. The role of collagen in cancer: from bench to bedside. Journal of Translational Medicine. 2019;17(1):309.
94. Taufalele PV, VanderBurgh JA, Munoz A, Zanotelli MR, Reinhart-King CA. Fiber alignment drives changes in architectural and mechanical features in collagen matrices. PLoS One. 2019;14(5):e0216537.
95. Nerger BA, Brun PT, Nelson CM. Microextrusion printing cell-laden networks of type I collagen with patterned fiber alignment and geometry. Soft Matter. 2019;15(28):5728-38.
96. Provenzano PP, Inman DR, Eliceiri KW, Trier SM, Keely PJ. Contact guidance mediated three-dimensional cell migration is regulated by Rho/ROCK-dependent matrix reorganization. Biophys J. 2008;95(11):5374-84.
97. Provenzano PP, Inman DR, Eliceiri KW, Knittel JG, Yan L, Rueden CT, et al. Collagen density promotes mammary tumor initiation and progression. BMC Med. 2008;6:11.
98. Duffy SW, Morrish OWE, Allgood PC, Black R, Gillan MGC, Willsher P, et al. Mammographic density and breast cancer risk in breast screening assessment cases and women with a family history of breast cancer. Eur J Cancer. 2018;88:48-56.
99. Potter M, Newport E, Morten KJ. The Warburg effect: 80 years on. Biochem Soc Trans. 2016;44(5):1499-505.
100. Mah EJ, Lefebvre A, McGahey GE, Yee AF, Digman MA. Collagen density modulates triple-negative breast cancer cell metabolism through adhesion-mediated contractility. Sci Rep. 2018;8(1):17094.

101. Seftor EA, Meltzer PS, Kirschmann DA, Margaryan NV, Seftor RE, Hendrix MJ. The epigenetic reprogramming of poorly aggressive melanoma cells by a metastatic microenvironment. J Cell Mol Med. 2006;10(1):174-96.
102. Franco-Barraza J, Beacham DA, Amatangelo MD, Cukierman E. Preparation of Extracellular Matrices Produced by Cultured and Primary Fibroblasts. Curr Protoc Cell Biol. 2016;71:10.9.1-.9.34.
103. Herculano-Houzel S, von Bartheld CS, Miller DJ, Kaas JH. How to count cells: the advantages and disadvantages of the isotropic fractionator compared with stereology. Cell Tissue Res. 2015;360(1):29-42.
104. Wisniewski JR, Zougman A, Nagaraj N, Mann M. Universal sample preparation method for proteome analysis. Nat Methods. 2009;6(5):359-62.
105. Merl J, Ueffing M, Hauck SM, von Toerne C. Direct comparison of MS-based label-free and SILAC quantitative proteome profiling strategies in primary retinal Muller cells. Proteomics. 2012;12(12):1902-11.
106. Hauck SM, Dietter J, Kramer RL, Hofmaier F, Zipplies JK, Amann B, et al. Deciphering membrane-associated molecular processes in target tissue of autoimmune uveitis by label-free quantitative mass spectrometry. Mol Cell Proteomics. 2010;9(10):2292-305.
107. Szklarczyk D, Gable AL, Lyon D, Junge A, Wyder S, Huerta-Cepas J, et al. STRING v11: protein-protein association networks with increased coverage, supporting functional discovery in genome-wide experimental datasets. Nucleic Acids Res. 2019;47(D1):D607-d13.
108. Feldman AT, Wolfe D. Tissue processing and hematoxylin and eosin staining. Methods Mol Biol. 2014;1180:31-43.
109. Sotgia F, Fiorillo M, Lisanti MP. Mitochondrial markers predict recurrence, metastasis and tamoxifen-resistance in breast cancer patients: Early detection of treatment failure with companion diagnostics. Oncotarget. 2017;8(40):68730-45.
110. dos Santos PB, Zanetti JS, Ribeiro-Silva A, Beltrao EI. Beta 1 integrin predicts survival in breast cancer: a clinicopathological and immunohistochemical study. Diagn Pathol. 2012;7:104.
111. Karnoub AE, Dash AB, Vo AP, Sullivan A, Brooks MW, Bell GW, et al. Mesenchymal stem cells within tumour stroma promote breast cancer metastasis. Nature. 2007;449(7162):557-63.
112. Karousou E, D'Angelo ML, Kouvidi K, Vigetti D, Viola M, Nikitovic D, et al. Collagen VI and hyaluronan: the common role in breast cancer. Biomed Res Int. 2014;2014:606458.
113. Park J, Scherer PE. Adipocyte-derived endotrophin promotes malignant tumor progression. J Clin Invest. 2012;122(11):4243-56.
114. Gordon MK, Hahn RA. Collagens. Cell Tissue Res. 2010;339(1):247-57.
115. Izu Y, Ansorge HL, Zhang G, Soslowsky LJ, Bonaldo P, Chu ML, et al. Dysfunctional tendon collagen fibrillogenesis in collagen VI null mice. Matrix Biol. 2011;30(1):53-61.
116. Ray G TM. Tenosynovitis. StatPearls Publishing. 2019 June.
117. Andia I, Rubio-Azpeitia E, Maffulli N. Platelet-rich plasma modulates the secretion of inflammatory/angiogenic proteins by inflamed tenocytes. Clin Orthop Relat Res. 2015;473(5):1624-34.
118. Iyengar P, Espina V, Williams TW, Lin Y, Berry D, Jelicks LA, et al. Adipocyte-derived collagen VI affects early mammary tumor progression in vivo, demonstrating a critical interaction in the tumor/stroma microenvironment. J Clin Invest. 2005;115(5):1163-76.
119. Willumsen N, Bager C, Karsdal MA. Matrix Metalloprotease Generated Fragments of Type VI Collagen Have Serum Biomarker Potential in Cancer - A Proof of Concept Study. Transl Oncol. 2019;12(5):693-8.
120. Cescon M, Gattazzo F, Chen P, Bonaldo P. Collagen VI at a glance. J Cell Sci. 2015;128(19):3525-31.
121. Bu D, Crewe C, Kusminski CM, Gordillo R, Ghaben AL, Kim M, et al. Human endotrophin as a driver of malignant tumor growth. JCI Insight. 2019;5.

122. Aldinucci D, Colombatti A. The inflammatory chemokine CCL5 and cancer progression. Mediators Inflamm. 2014;2014:292376.
123. Mira E, Lacalle RA, Gonzalez MA, Gomez-Mouton C, Abad JL, Bernad A, et al. A role for chemokine receptor transactivation in growth factor signaling. EMBO Rep. 2001;2(2):151-6.
124. Maillard L, Saito N, Hlawaty H, Friand V, Suffee N, Chmilewsky F, et al. RANTES/CCL5 mediated-biological effects depend on the syndecan-4/PKCα signaling pathway. Biol Open. 2014;3(10):995-1004.
125. Charnaux N, Brule S, Chaigneau T, Saffar L, Sutton A, Hamon M, et al. RANTES (CCL5) induces a CCR5-dependent accelerated shedding of syndecan-1 (CD138) and syndecan-4 from HeLa cells and forms complexes with the shed ectodomains of these proteoglycans as well as with those of CD44. Glycobiology. 2005;15(2):119-30.
126. Giordanengo V, Limouse M, Doglio A, Lesimple J, Lefebvre JC. Alteration of CD44 expression in HIV type 1-infected T cell lines. AIDS Res Hum Retroviruses. 1996;12(17):1615-22.
127. Michie CA, Tantscher E, Schall T, Rot A. Physiological secretion of chemokines in human breast milk. Eur Cytokine Netw. 1998;9(2):123-9.
128. Bottcher MF, Jenmalm MC, Bjorksten B, Garofalo RP. Chemoattractant factors in breast milk from allergic and nonallergic mothers. Pediatr Res. 2000;47(5):592-7.
129. Datar I, Qiu X, Ma HZ, Yeung M, Aras S, de la Serna I, et al. RKIP regulates CCL5 expression to inhibit breast cancer invasion and metastasis by controlling macrophage infiltration. Oncotarget. 2015;6(36):39050-61.
130. Soria G, Ben-Baruch A. The inflammatory chemokines CCL2 and CCL5 in breast cancer. Cancer Lett. 2008;267(2):271-85.
131. Khalid A, Wolfram J, Ferrari I, Mu C, Mai J, Yang Z, et al. Recent Advances in Discovering the Role of CCL5 in Metastatic Breast Cancer. Mini Rev Med Chem. 2015;15(13):1063-72.
132. Yaal-Hahoshen N, Shina S, Leider-Trejo L, Barnea I, Shabtai EL, Azenshtein E, et al. The chemokine CCL5 as a potential prognostic factor predicting disease progression in stage II breast cancer patients. Clin Cancer Res. 2006;12(15):4474-80.
133. Hartmann MC, Dwyer RM, Costello M, Potter SM, Curran C, Hennessy E, et al. Relationship between CCL5 and transforming growth factor-beta1 (TGFbeta1) in breast cancer. Eur J Cancer. 2011;47(11):1669-75.
134. Bieche I, Lerebours F, Tozlu S, Espie M, Marty M, Lidereau R. Molecular profiling of inflammatory breast cancer: identification of a poor-prognosis gene expression signature. Clin Cancer Res. 2004;10(20):6789-95.
135. Walens A, DiMarco AV, Lupo R, Kroger BR, Damrauer JS, Alvarez JV. CCL5 promotes breast cancer recurrence through macrophage recruitment in residual tumors. Elife. 2019;8.
136. Aldinucci D, Casagrande N. Inhibition of the CCL5/CCR5 Axis against the Progression of Gastric Cancer. Int J Mol Sci. 2018;19(5).
137. Norton KA, Wallace T, Pandey NB, Popel AS. An agent-based model of triple-negative breast cancer: the interplay between chemokine receptor CCR5 expression, cancer stem cells, and hypoxia. BMC Syst Biol. 2017;11(1):68.
138. Velasco-Velazquez M, Jiao X, De La Fuente M, Pestell TG, Ertel A, Lisanti MP, et al. CCR5 antagonist blocks metastasis of basal breast cancer cells. Cancer Res. 2012;72(15):3839-50.
139. Nan H, Liang L, Chen G, Liu L, Liu R, Jiao Y. Realizations of highly heterogeneous collagen networks via stochastic reconstruction for micromechanical analysis of tumor cell invasion. Physical Review E. 2018;97(3):033311.
140. Miyazaki K, Oyanagi J, Hoshino D, Togo S, Kumagai H, Miyagi Y. Cancer cell migration on elongate protrusions of fibroblasts in collagen matrix. Scientific Reports. 2019;9(1):292.
141. Hanahan D, Weinberg RA. Hallmarks of cancer: the next generation. Cell. 2011;144(5):646-74.

142. Truong D, Puleo J, Llave A, Mouneimne G, Kamm RD, Nikkhah M. Breast Cancer Cell Invasion into a Three Dimensional Tumor-Stroma Microenvironment. Scientific Reports. 2016;6(1):34094.
143. Seluanov A, Hine C, Azpurua J, Feigenson M, Bozzella M, Mao Z, et al. Hypersensitivity to contact inhibition provides a clue to cancer resistance of naked mole-rat. Proc Natl Acad Sci U S A. 2009;106(46):19352-7.
144. Conklin MW, Keely PJ. Why the stroma matters in breast cancer: insights into breast cancer patient outcomes through the examination of stromal biomarkers. Cell Adh Migr. 2012;6(3):249-60.
145. Campillo N, Falcones B, Otero J, Colina R, Gozal D, Navajas D, et al. Differential Oxygenation in Tumor Microenvironment Modulates Macrophage and Cancer Cell Crosstalk: Novel Experimental Setting and Proof of Concept. Front Oncol. 2019;9:43.
146. Zhang C, Wang S, Israel HP, Yan SX, Horowitz DP, Crockford S, et al. Higher locoregional recurrence rate for triple-negative breast cancer following neoadjuvant chemotherapy, surgery and radiotherapy. Springerplus. 2015;4:386.
147. van Roozendaal LM, Smit LHM, Duijsens G, de Vries B, Siesling S, Lobbes MBI, et al. Risk of regional recurrence in triple-negative breast cancer patients: a Dutch cohort study. Breast Cancer Res Treat. 2016;156(3):465-72.
148. Taroni P, Quarto G, Pifferi A, Abbate F, Balestreri N, Menna S, et al. Breast tissue composition and its dependence on demographic risk factors for breast cancer: non-invasive assessment by time domain diffuse optical spectroscopy. PLoS One. 2015;10(6):e0128941.
149. Steward LT, Gao F, Taylor MA, Margenthaler JA. Impact of radiation therapy on survival in patients with triple-negative breast cancer. Oncol Lett. 2014;7(2):548-52.
150. Kim CS AO. Radiation Therapy For Early Stage Breast Cancer. StatPearls Publishing. 2020.
151. Rave-Frank M, Virsik-Kopp P, Pradier O, Nitsche M, Grunefeld S, Schmidberger H. In vitro response of human dermal fibroblasts to X-irradiation: relationship between radiation-induced clonogenic cell death, chromosome aberrations and markers of proliferative senescence or differentiation. Int J Radiat Biol. 2001;77(12):1163-74.
152. Joshi SC, Khan FA, Pant I, Shukla A. Role of radiotherapy in early breast cancer: an overview. Int J Health Sci (Qassim). 2007;1(2):259-64.
153. Baaße A, Machoy F, Juerß D, Baake J, Stang F, Reimer T, et al. Radiation Sensitivity of Adipose-Derived Stem Cells Isolated from Breast Tissue. Int J Mol Sci. 2018;19(7).
154. Luan A, Duscher D, Whittam AJ, Paik KJ, Zielins ER, Brett EA, et al. Cell-Assisted Lipotransfer Improves Volume Retention in Irradiated Recipient Sites and Rescues Radiation-Induced Skin Changes. Stem Cells. 2016;34(3):668-73.
155. Azenshtein E, Luboshits G, Shina S, Neumark E, Shahbazian D, Weil M, et al. The CC chemokine RANTES in breast carcinoma progression: regulation of expression and potential mechanisms of promalignant activity. Cancer Res. 2002;62(4):1093-102.
156. Wang QM, Lv L, Tang Y, Zhang L, Wang LF. MMP-1 is overexpressed in triple-negative breast cancer tissues and the knockdown of MMP-1 expression inhibits tumor cell malignant behaviors in vitro. Oncol Lett. 2019;17(2):1732-40.
157. Chien YC, Liu LC, Ye HY, Wu JY, Yu YL. EZH2 promotes migration and invasion of triple-negative breast cancer cells via regulating TIMP2-MMP-2/-9 pathway. Am J Cancer Res. 2018;8(3):422-34.
158. Jiang H, Hegde S, DeNardo DG. Tumor-associated fibrosis as a regulator of tumor immunity and response to immunotherapy. Cancer Immunol Immunother. 2017;66(8):1037-48.
159. Araujo JM, Gomez AC, Aguilar A, Salgado R, Balko JM, Bravo L, et al. Effect of CCL5 expression in the recruitment of immune cells in triple negative breast cancer. Sci Rep. 2018;8(1):4899.
160. Rancoule C, Espenel S, Trone JC, Langrand-Escure J, Vallard A, Rehailia-Blanchard A, et al. Lysophosphatidic acid (LPA) as a pro-fibrotic and pro-oncogenic factor: a pivotal target to improve the radiotherapy therapeutic index. Oncotarget. 2017;8(26):43543-54.

161. Brooks D, Zimmer A, Wakefield L, Lyle LT, Difilippantonio S, Tucci FC, et al. Limited fibrosis accompanies triple-negative breast cancer metastasis in multiple model systems and is not a preventive target. Oncotarget. 2018;9(34):23462-81.
162. Bissell MJ, Radisky D. Putting tumours in context. Nat Rev Cancer. 2001;1(1):46-54.
163. Chen Y, He Y, Wang X, Lu F, Gao J. Adipose-derived mesenchymal stem cells exhibit tumor tropism and promote tumorsphere formation of breast cancer cells. Oncol Rep. 2019;41(4):2126-36.
164. Francis SL, Duchi S, Onofrillo C, Di Bella C, Choong PFM. Adipose-Derived Mesenchymal Stem Cells in the Use of Cartilage Tissue Engineering: The Need for a Rapid Isolation Procedure. Stem Cells Int. 2018;2018:8947548.
165. Minteer D, Marra KG, Rubin JP. Adipose-derived mesenchymal stem cells: biology and potential applications. Adv Biochem Eng Biotechnol. 2013;129:59-71.
166. Dwyer RM, Potter-Beirne SM, Harrington KA, Lowery AJ, Hennessy E, Murphy JM, et al. Monocyte chemotactic protein-1 secreted by primary breast tumors stimulates migration of mesenchymal stem cells. Clin Cancer Res. 2007;13(17):5020-7.
167. Escobar P, Bouclier C, Serret J, Bièche I, Brigitte M, Caicedo A, et al. IL-1β produced by aggressive breast cancer cells is one of the factors that dictate their interactions with mesenchymal stem cells through chemokine production. Oncotarget. 2015;6(30):29034-47.
168. Werts C, le Bourhis L, Liu J, Magalhaes JG, Carneiro LA, Fritz JH, et al. Nod1 and Nod2 induce CCL5/RANTES through the NF-kappaB pathway. Eur J Immunol. 2007;37(9):2499-508.
169. Dou Y, Jiang X, Xie H, He J, Xiao S. The Jun N-terminal kinases signaling pathway plays a "seesaw" role in ovarian carcinoma: a molecular aspect. J Ovarian Res. 2019;12(1):99.
170. Nakamichi K, Saiki M, Sawada M, Takayama-Ito M, Yamamuro Y, Morimoto K, et al. Rabies virus-induced activation of mitogen-activated protein kinase and NF-kappaB signaling pathways regulates expression of CXC and CC chemokine ligands in microglia. J Virol. 2005;79(18):11801-12.
171. Hass R, von der Ohe J, Ungefroren H. Potential Role of MSC/Cancer Cell Fusion and EMT for Breast Cancer Stem Cell Formation. Cancers (Basel). 2019;11(10).
172. Batlle R, Andres E, Gonzalez L, Llonch E, Igea A, Gutierrez-Prat N, et al. Regulation of tumor angiogenesis and mesenchymal-endothelial transition by p38alpha through TGF-beta and JNK signaling. Nat Commun. 2019;10(1):3071.
173. Ryan D, Paul BT, Koziol J, ElShamy WM. The pro- and anti-tumor roles of mesenchymal stem cells toward BRCA1-IRIS-overexpressing TNBC cells. Breast Cancer Res. 2019;21(1):53.
174. Tang CH, Hsu CJ, Fong YC. The CCL5/CCR5 axis promotes interleukin-6 production in human synovial fibroblasts. Arthritis Rheum. 2010;62(12):3615-24.
175. Fielding CA, Jones GW, McLoughlin RM, McLeod L, Hammond VJ, Uceda J, et al. Interleukin-6 signaling drives fibrosis in unresolved inflammation. Immunity. 2014;40(1):40-50.
176. Borthwick LA, Wynn TA, Fisher AJ. Cytokine mediated tissue fibrosis. Biochim Biophys Acta. 2013;1832(7):1049-60.
177. Choi I, Kang HS, Yang Y, Pyun KH. IL-6 induces hepatic inflammation and collagen synthesis in vivo. Clin Exp Immunol. 1994;95(3):530-5.
178. Ham IH, Oh HJ, Jin H, Bae CA, Jeon SM, Choi KS, et al. Targeting interleukin-6 as a strategy to overcome stroma-induced resistance to chemotherapy in gastric cancer. Mol Cancer. 2019;18(1):68.
179. Le TT, Karmouty-Quintana H, Melicoff E, Le TT, Weng T, Chen NY, et al. Blockade of IL-6 Trans signaling attenuates pulmonary fibrosis. J Immunol. 2014;193(7):3755-68.
180. Masjedi A, Hashemi V, Hojjat-Farsangi M, Ghalamfarsa G, Azizi G, Yousefi M, et al. The significant role of interleukin-6 and its signaling pathway in the immunopathogenesis and treatment of breast cancer. Biomed Pharmacother. 2018;108:1415-24.

181. He JY, Wei XH, Li SJ, Liu Y, Hu HL, Li ZZ, et al. Adipocyte-derived IL-6 and leptin promote breast Cancer metastasis via upregulation of Lysyl Hydroxylase-2 expression. Cell Commun Signal. 2018;16(1):100.
182. Seo BR, Bhardwaj P, Choi S, Gonzalez J, Andresen Eguiluz RC, Wang K, et al. Obesity-dependent changes in interstitial ECM mechanics promote breast tumorigenesis. Sci Transl Med. 2015;7(301):301ra130.
183. Jin K, Pandey NB, Popel AS. Simultaneous blockade of IL-6 and CCL5 signaling for synergistic inhibition of triple-negative breast cancer growth and metastasis. Breast Cancer Res. 2018;20(1):54.
184. Emmelkamp JM, Rockstroh JK. Maraviroc, risks and benefits: a review of the clinical literature. Expert Opin Drug Saf. 2008;7(5):559-69.
185. Sauter MA, Brett E, Muller CM, Machens HG, Duscher D. Novel Assay Analyzing Tropism between Adipose-Derived Stem Cells and Breast Cancer Cells Reveals a Low Oncogenic Response. Breast Care (Basel). 2019;14(5):278-87.
186. Garza RM, Paik KJ, Chung MT, Duscher D, Gurtner GC, Longaker MT, et al. Studies in fat grafting: Part III. Fat grafting irradiated tissue--improved skin quality and decreased fat graft retention. Plast Reconstr Surg. 2014;134(2):249-57.
187. Borrelli MR, Patel RA, Sokol J, Nguyen D, Momeni A, Longaker MT, et al. Fat Chance: The Rejuvenation of Irradiated Skin. Plast Reconstr Surg Glob Open. 2019;7(2):e2092.
188. Dixon JM, Thomas J, Kerr GR, Williams LJ, Dodds C, Kunkler IH, et al. A study of margin width and local recurrence in breast conserving therapy for invasive breast cancer. Eur J Surg Oncol. 2016;42(5):657-64.
189. Warpenburg MJ. Deep Friction Massage in Treatment of Radiation-induced Fibrosis: Rehabilitative Care for Breast Cancer Survivors. Integr Med (Encinitas). 2014;13(5):32-6.